frontiers in Marine Science

ORIGINAL RESEARCH
published: 29 May 2020
doi: 10.3389/fmars.2020.00375

Along-Path Evolution of Biogeochemical and Carbonate System Properties in the Intermediate Water of the Western Mediterranean

Katrin Schroeder[1], Stefano Cozzi[2], Malek Belgacem[1,3], Mireno Borghini[4], Carolina Cantoni[2], Sara Durante[2], Antonio Petrizzo[1], Annalisa Poiana[5,6] and Jacopo Chiggiato[1]*

[1] CNR-ISMAR, Venezia, Italy, [2] CNR-ISMAR, Trieste, Italy, [3] Department of Environmental Sciences, Informatics and Statistics, Università Ca' Foscari, Venezia, Italy, [4] CNR-ISMAR, La Spezia, Italy, [5] Dipartimento di Scienze Agroalimentari, Università degli Studi di Udine, Udine, Italy, [6] Dipartimento di Scienze della Vita, Università degli Studi di Trieste, Trieste, Italy

OPEN ACCESS

Edited by:
Frédéric Cyr, Fisheries and Oceans Canada, Canada

Reviewed by:
Yoana G. Voynova, Helmholtz Centre for Materials and Coastal Research (HZG), Germany
Marta Álvarez, Spanish Institute of Oceanography (IEO), Spain

***Correspondence:**
Katrin Schroeder
katrin.schroeder@ismar.cnr.it

Specialty section:
This article was submitted to Physical Oceanography, a section of the journal Frontiers in Marine Science

Received: *05 August 2019*
Accepted: *01 May 2020*
Published: *29 May 2020*

Citation:
Schroeder K, Cozzi S, Belgacem M, Borghini M, Cantoni C, Durante S, Petrizzo A, Poiana A and Chiggiato J (2020) Along-Path Evolution of Biogeochemical and Carbonate System Properties in the Intermediate Water of the Western Mediterranean. Front. Mar. Sci. 7:375. doi: 10.3389/fmars.2020.00375

A basin-scale oceanographic cruise (OCEANCERTAIN2015) was carried out in the Western Mediterranean (WMED) in summer 2015 to study the evolution of hydrological and biogeochemical properties of the most ubiquitous water mass of the Mediterranean Sea, the Intermediate Water (IW). IW is a relatively warm water mass, formed in the Eastern Mediterranean (EMED) and identified by a salinity maximum all over the basin. While it flows westward, toward and across the WMED, it gradually loses its characteristics. This study describes the along-path changes of thermohaline and biogeochemical properties of the IW in the WMED, trying to discriminate changes induced by mixing and changes induced by interior biogeochemical processes. In the first part of the path (from the Sicily Channel to the Tyrrhenian Sea), respiration in the IW interior was found to have a dominant role in determining its biogeochemical evolution. Afterward, when IW crosses regions of enhanced vertical dynamics (Ligurian Sea, Gulf of Lion and Catalan Sea), mixing with surrounding water masses becomes the primary process. In the final part of the investigated IW path (the Menorca-Mallorca region), the role of respiration is further masked by the effects of a complex circulation of IW, indicating that short-term sub-regional hydrological processes are important to define IW characteristics in the westernmost part of the investigated area. A pronounced along-path acidification was detected in IW, mainly due to remineralization of organic matter. This induced a shift of the carbonate equilibrium toward more acidic species and makes this water mass increasingly less adequate for an optimal growth of calcifying organisms. The carbonate buffering capacity also decreases as IW flows through the WMED, making it more exposed to the adverse effects of a decreasing pH. The present analysis indicates that IW evolution in the sub-basins of the WMED is currently driven by complex hydrological and biogeochemical processes, which could be differently impacted by coming climate changes, in particular considering expected increases of extreme meteorological events, mainly due to the warming of the Mediterranean basin.

Keywords: thermohaline circulation, mixing, mineralization layer, nutrients, ocean acidification, climate change

INTRODUCTION

The Mediterranean Sea is an elongated basin between Europe and Africa, with restricted communications with the Atlantic Ocean, the Black Sea and the Red Sea. The two main subbasins composing it, the Eastern Mediterranean (EMED) and the Western Mediterranean (WMED), are separated by the relatively shallow Sicily Channel (540 m depth). It is well known that major oceanic processes take place in the Mediterranean, though on smaller scales than those occurring in the oceans (Millot and Taupier-Letage, 2005; Schneider et al., 2010; Schroeder et al., 2012). The most prominent example is the role that dense water formation (DWF) events have in the basin-wide circulation cell, which is a miniature version of the oceanic conveyor belt (Schroeder et al., 2012).

In the Mediterranean, the thermohaline circulation forms an open cell, starting in the Strait of Gibraltar with an inflow of Atlantic Water (AW) and ending at the same strait with an undercurrent outflow of intermediate and deep Mediterranean water masses (Astraldi et al., 1999; Millot, 1999). This cell is driven by regional climatic conditions, which cause net buoyancy fluxes toward the atmosphere and by freshwater deficits, due to the excess of evaporation compared to precipitation and runoff (Lionello et al., 2006). The relatively fresh AW flows mainly eastward, in an upper layer that slowly erodes, such that its core progressively modifies along the southern coast and through the Sicily Channel into the EMED, where it eventually disappears (Millot, 1999). Except for this thin layer, the Mediterranean Sea is filled with Mediterranean water. The transformation of AW by air-sea heat and freshwater fluxes leads to the formation of distinct Intermediate and Deep Waters (IW and DW, respectively). IW forms in the EMED and resides at depths from which it can flow through the Sicily Channel into the WMED, whereas the deep circulation cells are separated by the topographic constraints of the channel, with Western Mediterranean Deep Water (WMDW) filling up the deep WMED and Eastern Mediterranean Deep Water (EMDW) filling up the deep EMED (Astraldi et al., 1999; Millot and Taupier-Letage, 2005; Schneider et al., 2010; Schroeder et al., 2012, 2017).

IW forms via salinification and densification of surface waters in the Levantine Basin (Levantine Intermediate Water, LIW) and in the Cretan Sea (Cretan Intermediate Water, CIW) (Millot and Taupier-Letage, 2005; Schroeder et al., 2017). After sinking to its equilibrium depth (100–800 m), IW spreads throughout the whole Mediterranean Sea (Lascaratos et al., 1993). The core of this water mass can be easily identified by an absolute maximum in salinity and by a relative maximum in temperature in the water column (Schroeder et al., 2017; Millot, 2013).

From a hydrological point of view, IW can be considered a useful oceanographic proxy as it is modulated by a variety of processes: DWF in the Gulf of Lion (Schroeder et al., 2006; Testor et al., 2018) and in the Adriatic Sea (Gačić et al., 2001; Chiggiato et al., 2016), interaction with mesoscale structures (Algerian Eddies, Cotroneo et al., 2016), mixing with EMDW and cascading in the Tyrrhenian Sea (Sparnocchia et al., 1999) and double diffusive phenomena in the Tyrrhenian Sea (Durante et al., 2019). IW is crucial in determining the thermohaline characteristics of the deep Mediterranean water (Schroeder et al., 2006) and it responds to long- and short-term climatic changes in the Mediterranean (Toucanne et al., 2012; Schroeder et al., 2017). On a larger perspective, IW also constitutes the bulk of the salty and warm outflow from the Gibraltar Strait (∼1 Sv), which exerts an influence on present thermohaline properties of the North Atlantic Ocean (Voelker et al., 2006). Thermohaline changes of oceanic intermediate waters are thought to be important for the understanding of climatic oscillations and trends worldwide (Arabic and Owens, 2001). Similarly, physical changes of Mediterranean IW can be considered a useful proxy to infer the effects of regional climate changes.

From a biogeochemical point of view, anthropogenic activities have already impacted all water masses in the Mediterranean, including IW (The MERMEX Group, 2011). Biogeochemical elements distribution in this basin is mainly driven by water exchanges through the straits (Huertas et al., 2012), continental inputs (Ludwig et al., 2009) and atmospheric deposition (Markaki et al., 2010), which overall induce a stoichiometric excess of nitrogen with respect to phosphorus and silicon (Schroeder et al., 2010). The Mediterranean Sea currently exhibits a basin-scale west-to-east gradient of oligotrophy that is concomitant with the west-to-east decline of phosphorus availability (Pujo-Pay et al., 2011; Krom et al., 2014).

Along the path through the Mediterranean Sea, IW becomes progressively a water mass that is nutrient-enriched, poor in dissolved organic matter (DOM) and undersaturated with respect to dissolved oxygen, because of the preponderance of mineralization in the layers below the deep chlorophyll maximum (DCM; 40–80 m in the WMED, and 80–100 m in the EMED; Pujo-Pay et al., 2011). However, it is expected that complex modifications of the biogeochemistry of IW might occur in the future, as a result of climate change, and mainly due to: (i) alteration of the runoff and of atmospheric deposition in the Mediterranean drainage basin, (ii) changes of chemical characteristics of coastal and open-sea upper waters involved in DWF events, (iii) regional changes of productivity and of the sedimentation of biogenic particulate in the mineralization layer, and (iv) changes in the structure and/or distribution along the water column of microbial communities (The MERMEX Group, 2011; Pujo-Pay et al., 2011; Krom et al., 2014).

IW is also a key water mass to understand the decadal variability of carbonate system properties in the Mediterranean Sea (Palmiéri et al., 2015). The capability to absorb atmospheric CO_2 per unit of surface is relatively high in the Mediterranean compared to the global ocean for two main reasons: a shorter ventilation time scale of its bottom waters (Schneider et al., 2014; Stöven and Tanhua, 2014) and a higher total alkalinity that favors the dissolution of air CO_2 (Álvarez et al., 2014b). Carbon sequestration in this basin follows two main pathways, both linked to the IW: (i) the CO_2 absorption and export during DWF events (physical carbon pump) in winter (Touratier et al., 2016; Cantoni et al., 2016) and (ii) the photosynthetic uptake of CO_2 and its subsequent release at depth during remineralization of sinking organic matter (Bethoux et al., 2005), which mostly occurs within the IW (biological carbon pump). The anthropogenic CO_2 has already penetrated the whole water

column of the Mediterranean Sea (Schneider et al., 2010; Palmiéri et al., 2015; Hassoun et al., 2015; Sisma-Ventura et al., 2016). This has led to a decrease of pH and carbonate ion concentration in seawater, a process known as ocean acidification (Hassoun et al., 2015; Álvarez et al., 2014b). Its impact on Mediterranean ecosystems is still difficult to predict, despite the great effort made in the last decades, as it could interact with other stressors like the warming of Mediterranean water (Adloff et al., 2015; Lacoue-Labarthe et al., 2016; Milner et al., 2016).

Time scales of water mass formation and spreading through the Mediterranean are a basic factor that determines the response of the different water masses to the modifications of climatic conditions, since dense waters are in contact with the atmosphere only during their formation at a few locations (Arabic and Owens, 2001). The Mediterranean Sea has a relatively fast overturning circulation compared to the oceans. A residence time of water masses of up to ∼150 years was estimated for the entire basin, with the longest time being reached in the EMDW, which is isolated by its bottom topography (Schneider et al., 2010, 2014). Stratford et al. (1998) estimated a deep water renewal time of 20–40 years for the WMED and Roether et al. (1996) of about 70–150 years for the EMED. Therefore, all water masses in the Mediterranean have already been exposed to the increase of atmospheric CO_2 occurred since the beginning of the industrial age. However, a weak accuracy in the estimates of ventilation ages of specific Mediterranean water masses still persists, mainly due to their non-steady-state, which is a key requirement for this analysis (Schneider et al., 2010; Stöven and Tanhua, 2014). Concerning IW, Schneider et al. (2010) estimated a mean age of 50–60 years in the Sicily Channel, a value that indicates that the evolution of IW in the WMED can be a useful indicator of the coupling between oceanographic processes and climatic forcings on a multi-decadal scale.

Thermohaline properties and circulation of water masses in the Mediterranean depend on climatic conditions that, although largely forced by planetary scale patterns, show an important regional variability (Lionello et al., 2006; Giorgi, 2006). In this basin, multi-decadal trends of precipitation decrease and air temperature increase were detected, together to an increase of short-term extreme events like storms, heavy rainfall, heatwaves (The MERMEX Group, 2011; Drobinski et al., 2018; Darmaraki et al., 2019b). As a consequence, long and short-term physical changes were observed in the Mediterranean Sea like the transitions in the thermohaline characteristics in the eastern (Eastern Mediterranean Transient, EMT, Roether et al., 1996) and in the western (Western Mediterranean Transition, WMT, Schroeder et al., 2016) basin. The Mediterranean Sea underwent a general warming during the last 50 years that affected all water masses (Lionello et al., 2006; Bindoff et al., 2007). In the Sicily Channel, IW showed increases of 0.024°C yr^{-1} and 0.006 yr^{-1} in θ and S, respectively, during the last 2 decades (Schroeder et al., 2017). Anomalous heatwaves in large regions of the Mediterranean basin caused high SST in 2003 (Olita et al., 2007) and in most recent years (Bensoussan et al., 2019; Darmaraki et al., 2019a).

Considering the importance of IW as a proxy of thermohaline, biogeochemical and carbonate system transformations in the Mediterranean Sea, this study aims to better understand its evolution across the WMED. The biogeochemical properties of seawater are determined by the mixing among different water masses (a conservative process), and by physico-chemical or biological transformations acting in the interior of the water mass (non-conservative processes). Here, the results of a multiparametric mixing analysis are used to assess the roles of mixing with surrounding waters and of internal biogeochemical processes, in order to draw attention to the potential evolution that IW may experience as a consequence of climate change.

The study is based on the dataset collected during the cruise OCEANCERTAIN 2015 (OC2015), carried out in August 2015, which was focused on investigating the water mass circulation in the sub-basins of the WMED (**Figure 1**).

MATERIALS AND METHODS

Experimental Design

The OC2015 cruise was designed according to the results from past cruises and scientific literature (Schroeder et al., 2012). Its purpose was to intercept the flow of IW across the different WMED sub-basins (**Figure 1**) and to observe its transformation.

CTD Casts and Seawater Sampling

The OC2015 cruise was carried out with the R/V Minerva Uno, from August 4 to 31, 2015. CTD downcasts were acquired at 92 stations. At each station, pressure (dbar), temperature (°C, SBE-3/F thermistor, Sea-Bird Scientific, Bellevue, WA, United States), conductivity (mS cm^{-1}, SBE-4 sensor Sea-Bird Scientific, Bellevue, WA, United States) and dissolved oxygen concentration (DO; μmol kg^{-1}, SBE-43 sensor, Sea-Bird Scientific, Bellevue, WA, United States) were measured with a CTD SBE 911 plus General Oceanics Rosette System (General Oceanics, Miami, FL, United States), equipped with 24 12-liters Niskin Bottles. Salinity (S) and potential temperature (θ; °C) were calculated by Sea-Bird Scientific routines. CTD profiles of all parameters were obtained by sampling the signals at 24 Hz, during the downcasts at a speed of 1 m s^{-1}, and processed on board.

Seawater samples (n = 550) for the determination of biogeochemical parameters were collected from the Niskin bottles. Samples for DO were drawn in 60-mL BOD bottles and treated with Winkler reagents immediately after collection. Samples for the determination of major nutrients (nitrate, NO_3^-; nitrite, NO_2^-; reactive silicate, SiO_2; orthophosphate, PO_4^{3-}; ammonium, NH_4^+; μmol l^{-1}), dissolved organic carbon (DOC, μmol l^{-1}) and total dissolved nitrogen (TDN, μmol l^{-1}) were syringe filtered using pre-combusted (450°C, 4 h) GF/F filters and placed in HDPE vials (previously cleaned and acid-conditioned). Afterward, the samples were quickly frozen at −20°C until the analysis. For the determination of pH on the total hydrogen ion scale at 25°C (pH_{T25}), the samples were drawn after DO samples into 10 cm long cylindrical glass cells and analyzed spectrophotometrically. For the determination of total alkalinity (TA; μmol kg^{-1}), the samples were collected in 300 ml borosilicate bottles, poisoned with mercuric chloride,

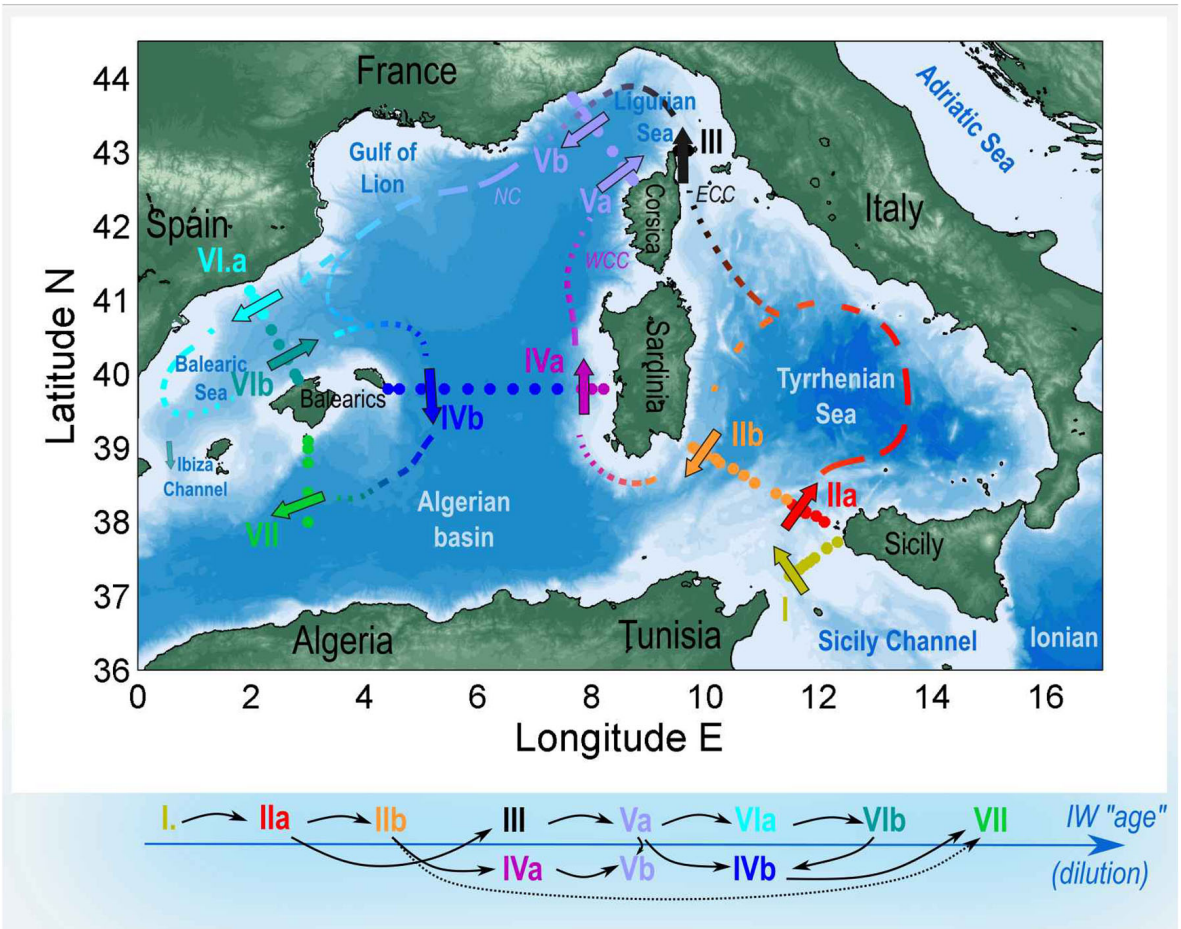

FIGURE 1 | Map of OC2015 cruise in August 2015, with a sketch of the IW path from the Sicily Channel to the interior of the western sub-basins. Colored areas and roman numbers (defined by physical data analysis and available literature) indicate the main path of IW in the WMED.

tightly closed and stored in the dark at a temperature similar to that one *in situ* (4–25°C).

Laboratory Methods

DO samples were analyzed on board by Winkler method (Grasshoff et al., 1999) with an automated potentiometric titration system Metrohm 798 MPT Titrino (CV = 0.17% at 215 μmol kg^{-1}), within 6 h after the sampling. They were used to post-calibrate CTD profiles of DO and to calculate apparent oxygen utilization (AOU; Benson and Krause, 1984). The determination of inorganic nutrients was carried out following standard colorimetric methods (Grasshoff et al., 1999) using an OI-Analytical flow-segmented autoanalyzer (Flow Solution III). The concentration of dissolved inorganic nitrogen (DIN) was calculated as $NO_3^- + NO_2^- + NH_4^+$.

Samples for the determination of DOC and TDN were analyzed by High-Temperature Catalytic Oxidation method, using a Shimadzu TOC-V analyzer equipped with a total nitrogen module (TNM-1) and an ASI-V autosampler (Grasshoff et al., 1999). DOC was determined by non-dispersive infrared method against four-point calibration curves obtained with potassium hydrogen phthalate solutions ($r^2 > 0.999$), following Grasshoff et al. (1999). TDN was determined by chemiluminescence, against three-point calibration curves obtained with potassium nitrate solutions ($r^2 > 0.999$). The precision of the analysis was 0.5 μmol C l^{-1} and 0.2 μmol N l^{-1} for DOC and TDN, respectively. Total system blank (1.5 μM C for DOC, undetectable for TDN) and the efficiency of the oxidation step were checked daily by the analysis of ultra-pure Millipore Q water and standard solutions. The concentration of dissolved organic nitrogen (DON) was calculated as TDN – DIN.

The carbonate system in seawater is defined by six variables: pH, total dissolved inorganic carbon (TCO_2), TA, partial pressure of CO_2 (pCO_2), concentration of bicarbonate (HCO_3^-) and carbonate (CO_3^{2-}) ions. Only two of these variables are needed to calculate the others, if θ, S and nutrient concentration *in situ* are known. pH_{T25} was measured on board, within 24 h after the sampling, using the spectrophotometric method with m-cresol purple as indicator (Clayton and Byrne, 1993). The precision was ±0.002 units ($n = 3$), accuracy and stability of the method were checked daily with reference seawater certified for TA and TCO_2 ($n = 34$, CRM batch 146 provided by Prof A. G. Dickson, Scripps,

California). TA was determined by potentiometric titration in an open cell with a difference derivative readout (Hernandez-Ayon et al., 1999). The average precision was ±2.0 μmol kg^{-1} (n = 86 duplicate samples) and the accuracy was checked daily by the titration of certified reference seawater (n = 59 CRM batch 146). TA and pH_{T25} data were used to calculate the other carbonate system parameters at *in situ* conditions, using CO2SYS program (Lewis and Wallace, 1998), with the constants from Mehrbach et al. (1973) as refit by Dickson and Millero (1987); Dickson (1990) for sulphates and Uppström (1974) for borate.

Data Processing and Mixing Analysis

Biogeochemical characteristics of IW along the different transects were analyzed by non-parametric statistics, whereas the significance of their along-path changes was assessed by the Mann–Whitney U test (Z, p).

The mixing among Water Types (WTs) in each sample of IW was estimated by an optimum multiparameter analysis (OMP; Tomczak and Large, 1989; Álvarez et al., 2014a). This analysis assumes that the mixing is a linear process that affects in the same way all considered seawater properties. For this reason, the contributions of (m) WTs to each sample can be assessed defining an equal number of seawater properties and solving a system of (m + 1) linear mixing equations (i.e. one equation for each property plus mass conservation equation). Given that this system does not have an exact solution, the best mixing combination is obtained through the minimization of the residuals in parameter space in a non-negative least squares sense.

Here, three WTs were defined by average values of θ and S (**Table 1**). For IW, they referred to the core of intermediate layer from publicly available datasets upstream (east of) subregion I. For AW, they were calculated from the 2015 data in the mixed layer from 40 to 150 m depth in the subregions (VII, I and IIa) that are directly affected by the inflow of surface waters from the Strait of Gibraltar. For DW, they were calculated from the 2015 data in the deeper layer (600–1000 m) along the main spreading pathway of deeper waters formed in the Gulf of Lion (IV to VII).

The set of mixing equations to solve is $A * X = N$, where A is the (4 × 3) matrix with the WT characteristics, X is the (3×n) matrix with the WT fractions, N is the (4×n) matrix with the measured variables, n being the number of samples. The linear equations are normalized and weighted. The normalization is done using the mean and standard deviation values for the three parameters in the WT matrix. Equations are weighted, considering the standard deviation of each parameter in the WT matrix and its uncertainty when estimating it. Weights of 8, 7, 5, and 10 were assigned to θ, S, DO and mass, respectively. As a result, all samples (**Figures 2A,B**) in the intermediate layer, downstream the region of the Sicily Channel, can be considered composed by these three WTs, with percentages that vary along the path of this water mass in the WMED. **Figures 2C,D** show the overall results of this analysis, with the vertical profiles of the mixing fractions of the three WTs in each subregion defined in **Figure 1**, and the total mass residuals vertical profiles.

The OMP showed the along-path mixing of IW with a decrease of IW fraction from 93% down to 34% at its core (**Table 4** and **Figure 2B**). This trend is consistent with those observed for hydrological and biogeochemical parameters (as shown later on when **Figures 3**, **4** are discussed). The mixing analysis was characterized by small mass residuals (<4%) in the intermediate layer. Outside, the residuals increased above 100 m (25%) up to 40% near the surface (**Figure 2D**).

TABLE 1 | Properties of Water Types (WTs) for AW, IW, and DW.

WTs (color in Figure 2A)	θ (°C)	S
WT_AW (green)	14.1	37.91
WT_IW (red)	14.865	38.915
WT_DW (cyan)	12.75	38.44

STUDY SITE DESCRIPTION

In the following, a general description of the oceanographic properties of the WMED during the OC2015 cruise is given, comprising the water masses that are not specifically analyzed in this study. The whole dataset of the cruise is analyzed in the cruise report Deliverable D2.12/2016 (Ocean-Certain FP7 project) and is published in Belgacem et al. (2019, under review) and in Cantoni et al. (2020, under review).

Thermohaline Properties of WMED Waters

In summer 2015 the upper layer of the WMED was characterized by the presence of relatively fresh (S = 37.25–38.25) and warm (15–30°C) AW, a consequence of the heatwave observed in the region in this year (Duchez et al., 2016). The layer occupied by AW extended from surface down to 100–200 m depth, depending on the region. Coherently with the main known circulation patterns in the WMED, the highest S in the AW layer was observed where this water was the eldest, in IIb, Vb and VI (**Figure 1**).

The IW is identified by a relative maximum in θ and absolute maximum in S from its origin in the Levantine basin and in the Cretan Sea, where the so-called Levantine Surface Water (LSW) becomes salty and warm before undergoing convection at specific sites (Schroeder et al., 2017). In 2015, IW was observed in the WMED at intermediate depths, between 100–200 m and 500–600 m, with S (38.55 to 38.90) and θ (13.2 to 15.0°C) values that significantly varied along its path through the basin.

The WMDW forms in the Algero-Provencal Basin (offshore the Gulf of Lion and within the Ligurian Sea) via deep convection and dense shelf water cascading, both processes involving AW and IW (Testor et al., 2018). During OC2015, S and θ of WMDW decreased from 600 m to the bottom from 38.47 to 38.70 and from 12.9°C to 13.7°C, respectively. As S and θ of both AW and IW have increased with time over the past decades, also the resulting WMDW has been found to increase its heat and salt content over time (Schroeder et al., 2016). The saltiest and warmest DW is generally found within the Tyrrhenian Sea (Astraldi and Gasparini, 1995). In summer 2015 it was detected in IIb, from

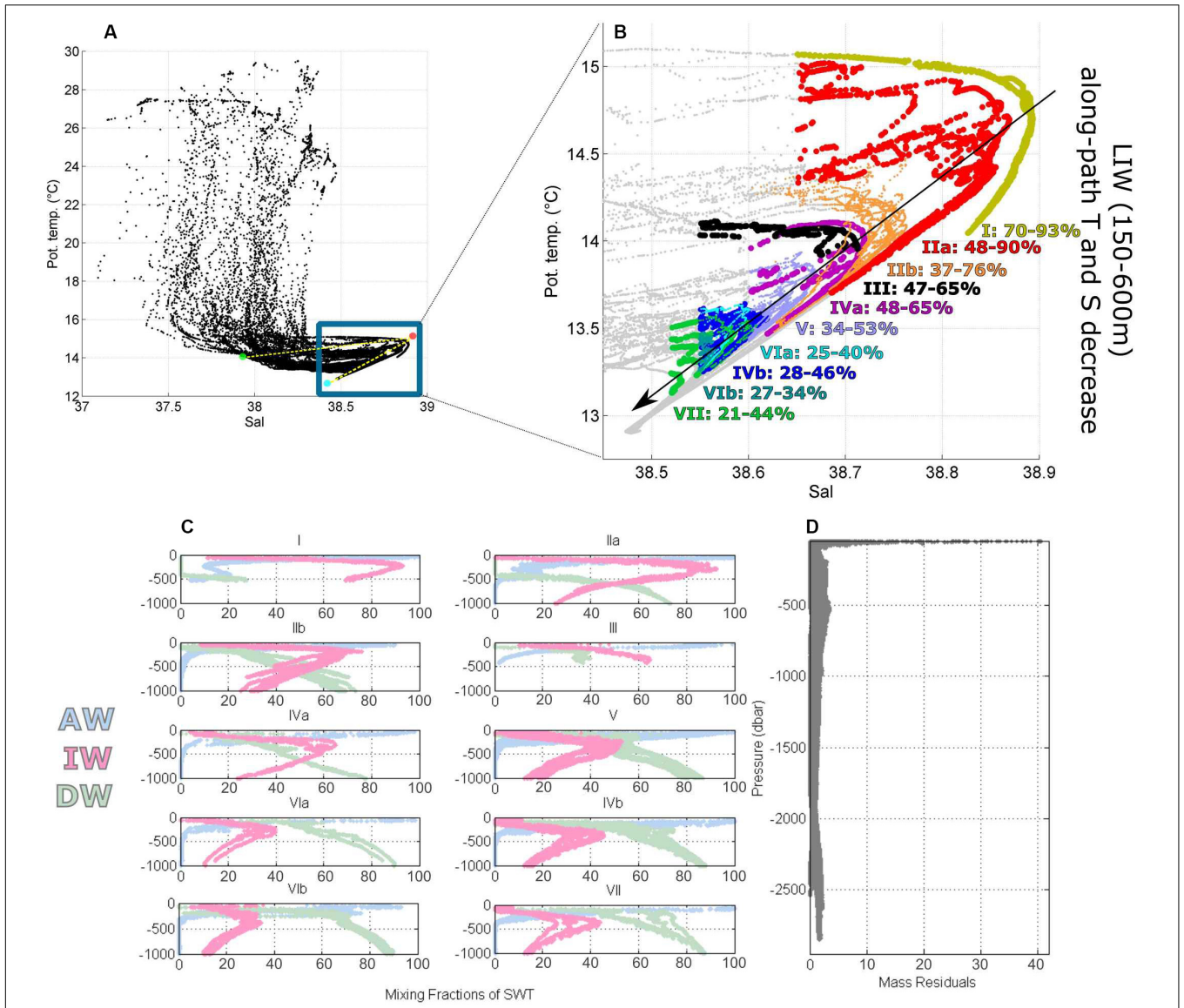

FIGURE 2 | (A) θS diagram of the OC2015 cruise, and **(B)** zoom on the intermediate and deep layer. In **(A)** the three colored dots indicate the θS properties of AW (green), IW (red) and DW (blue) used for the OMP analysis (**Table 1**), yellow dashed lines represent the mixing lines between IW and AW, and between IW and DW. In **(B)** colored dots within the IW layer (150–600 m + additional salinity constraints) are shown according to colored transects in **Figure 1**. Gray dots do not belong to IW. In addition, the percentage of IW within the core in each area is shown. **(C)** Vertical profiles of %AW, %IW and %DW in the different subregions; **(D)** vertical profile of mass residuals combining the results of the whole cruise.

where it exits from the Tyrrhenian as a mixing product between IW and WMDW (the so-called Tyrrhenian Deep Water, TDW).

Biogeochemical Properties of WMED Waters

From the biogeochemical point of view, the WMED is a meso- to oligo-trophic region, mainly characterized by a vertical displacement of a biogenic, mineralization and deep layer (The MERMEX Group, 2011; Pujo-Pay et al., 2011). In 2015, the upper layer (down to 100 m), where the deep chlorophyll maximum (DCM) is located, was characterized by a high concentration of DO (180–285 μM) and by low concentrations of nutrients (DIN < 4 μM, PO_4^{3-} < 0.14 μM, SiO_2 < 3.8 μM). In this layer, the depletion of inorganic nutrients was coupled to the highest concentrations of DOC and DON (up to 215 μM and 15 μM, respectively), that accumulate in the euphotic layer because of the prevalence of primary production over remineralization. Below, inorganic nutrients progressively increased with depth, down to 200 m for NO_{3-} and PO_4^{3-} and down to 500 m for SiO_2. DOC and DON decreased in correspondence to the nutricline, due to the prevalence of remineralization vs. primary production, which was also indicated by the positive values of AOU in all stations below 50–100 m depth.

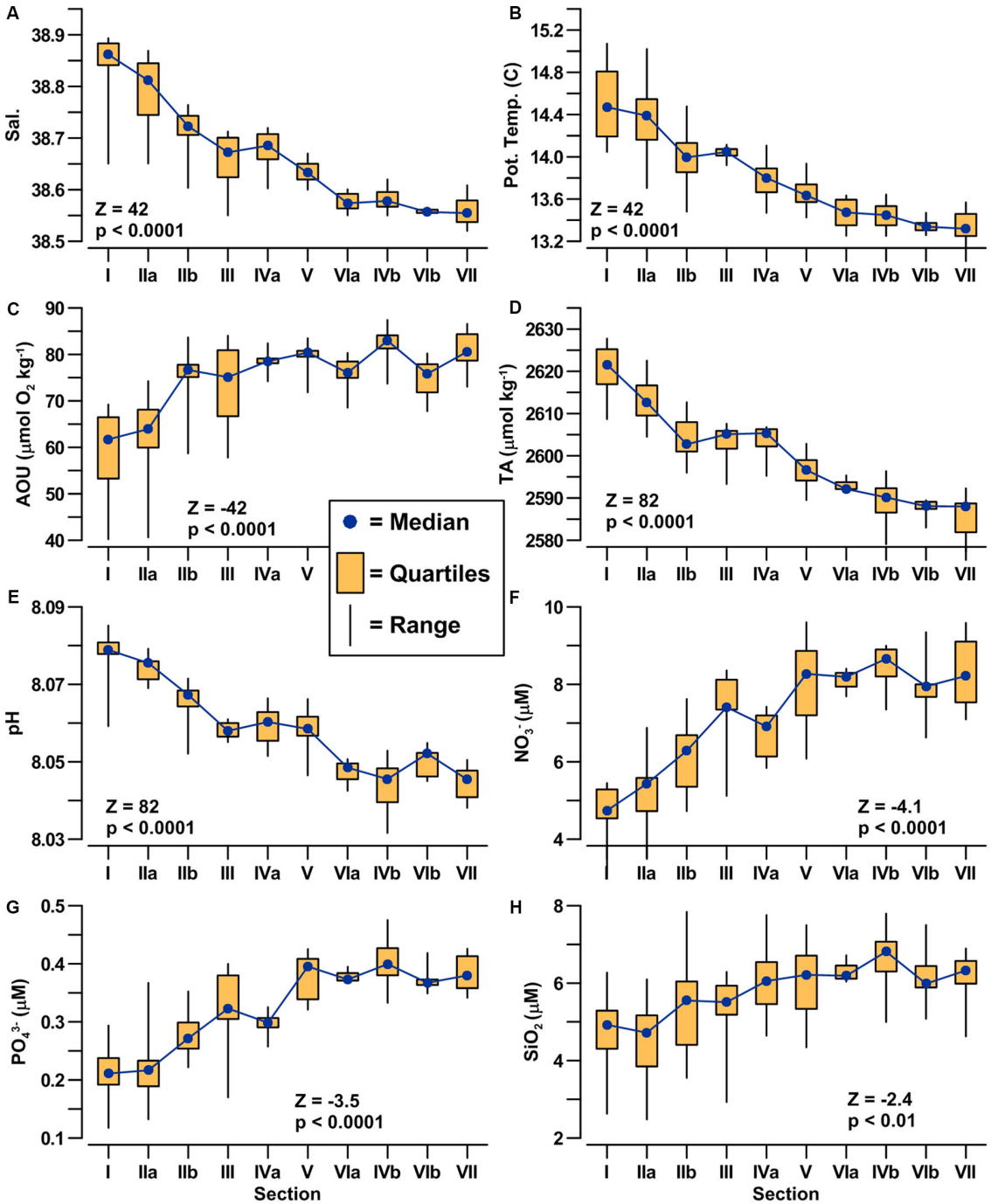

FIGURE 3 | Box-Whisker plots (median, quartiles, range of values) of IW properties in the subregions defined in **Figure 1**. The significance of the changes between the subregions I and VII (Mann–Whitney U test; Z value, probability) is also shown. **(A)** Salinity, **(B)** potential temperature, **(C)** apparent ocygen utilization, **(D)** total alkalinity, **(E)** pH, **(F)** nitrate, **(G)** phosphate, and **(H)** silicate.

In the WMED, the largest changes of TA and TCO_2 are observed in the AW and IW layers Álvarez et al., 2014b). In 2015 the lowest TA values (down to 2445 µmol kg^{-1}) were recorded in the upper layer of VII, where the fraction of AW was high, whereas the highest TA values were measured within the core of the IW at I (up to 2627 µmol kg^{-1}). For TCO_2 the lowest values were found in the upper layer of VII (down to 2128 µmol kg^{-1}), while values up to about 2340 µmol kg^{-1} were measured in the IW and DW. Contrary to TA, TCO_2 is strongly affected by air-sea CO_2 fluxes, photosynthesis and respiration. The small

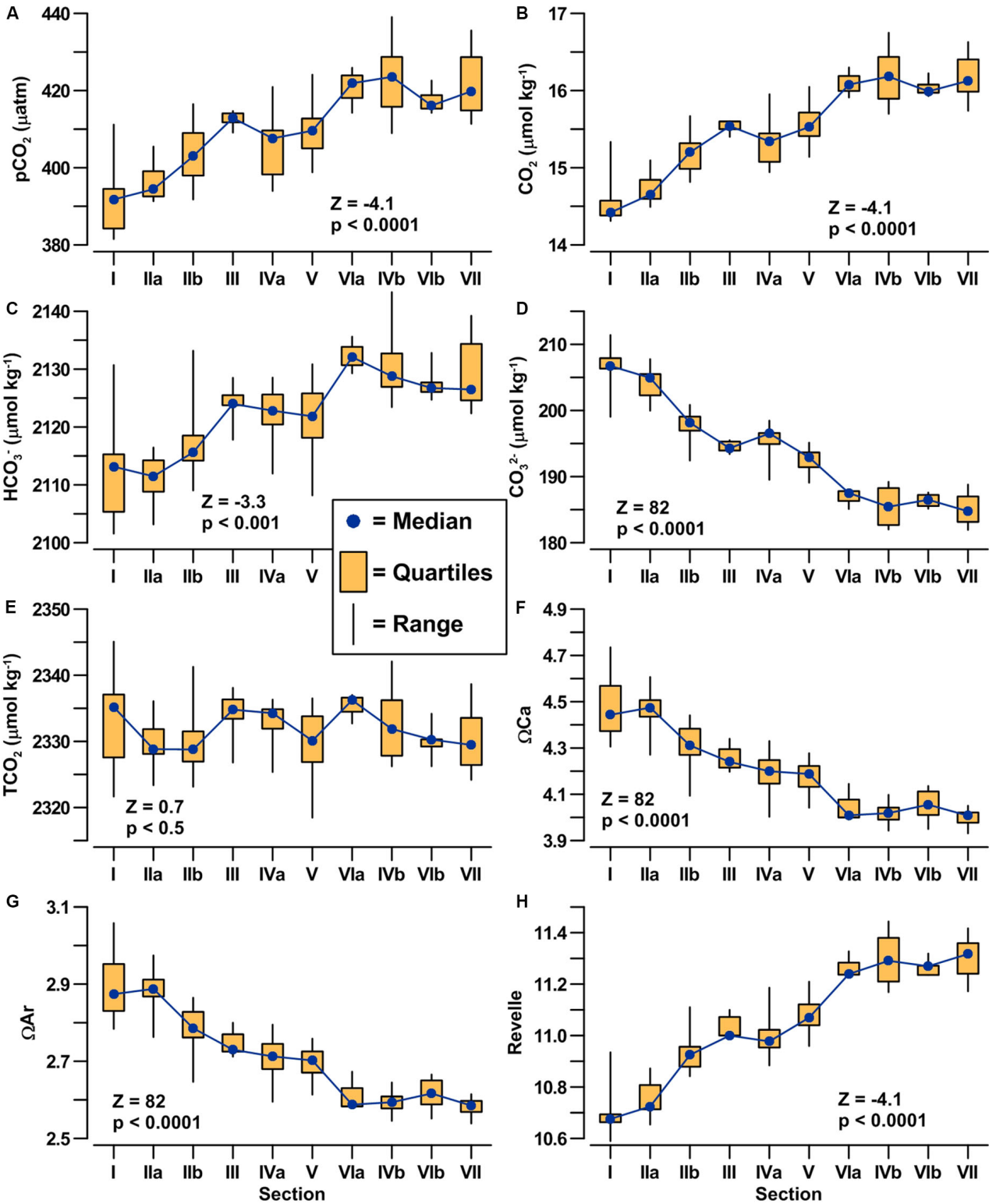

FIGURE 4 | Box-Whisker plots (median, quartiles, range of values) of IW properties (in the subregions defined in **Figure 1**. The significance of the changes between the subregions I and VII (Mann–Whitney U test; Z value, probability) is also shown. **(A)** pCO2, **(B)** CO_2, **(C)** HCO_3^-, **(D)** CO_3^{2-}, **(E)** TCO_2, **(F)** saturation state of calcite (ΩCa), **(G)** saturation state of aragonite (ΩAr), and **(H)** Revelle factor.

variability of surface TCO_2 with respect to the underneath water column suggests that both photosynthesis and CO_2 outgassing to the atmosphere (sea surface $pCO_2 > 400$ μatm in the whole region) contributed to maintain low TCO_2 levels.

IW Path Through the WMED

From previous studies (e.g. Schroeder et al., 2012) it is well known that after crossing the Sicily Channel (I, see **Figure 1**), through a narrow channel that allows exchanges of waters deeper than 200 m, IW turns right due to topographic constraints and its flow is diverted toward the Tyrrhenian Sea (on the Sicilian side of the transect Sardinia-Sicily, IIa). This subbasin is characterized by a cyclonic circulation and the IW may exit either through the southern opening (on the Sardinian side of IIb) or through the northern opening, the Corsica Channel (III). The IW vein that enters the Algerian basin through IIb, driven by the general cyclonic circulation, is diverted toward the north and crosses the transect between the Balearic Islands and Sardinia (on its Sardinian side, IVa), to proceed further northward and eventually cross the transect between France and Corsica (on its Corsican side, Va). This vein is part of the Western Corsica Current (WCC). The mainly northward flow through the Corsica Channel (III), which involves both the surface and the intermediate layers, is called the Eastern Corsica Current (ECC). When reaching the Ligurian Sea, the ECC joins the WCC to form the Northern Current (NC). This is the major cyclonic current that transports water westward along the northern shore of the WMED, crossing the transect between France and Corsica (on its continental side, Vb) and then the transect between Spain and Mallorca (on its continental side, VIa). Within the Balearic Sea, AW and IW may partially continue south-westward, through the Ibiza Channel (while DW cannot because of the shallowness of the channel), directly reaching the Alboran Sea, but most of IW turns cyclonically (Schroeder et al., 2008) and exits on the Balearic side of the Spain-Mallorca transect (VIb), to cross immediately after the Balearic side of the Menorca-Sardinia transect (IVb). From here the IW may reach the western Algerian basin and eventually the Alboran Sea, after crossing the transect between Mallorca and Algeria (VII).

RESULTS

In the following sections, thermohaline (θ and S) and biogeochemical properties are used to describe the evolution of IW along its path in the WMED and the potential implications of these changes. Afterward, the respective roles of mixing and biological processes are determined by using the OMP results.

Observed Along-Path Changes in the IW

A gradual evolution of IW thermohaline properties was observed across the WMED, from the Sicily Channel to the Balearic Sea, because of a progressive mixing with WMED water masses that causes a decreases of θ and S from I to VIa (**Figures 1**, **2B**, **3A,B**). Since the core of IW is characterized by a maximum in θ and S, as described earlier, mixing with surrounding waters leads to a concomitant decrease in θ and S during its pathway through the WMED. Median values of S and θ decrease from 38.86 and 14.47°C to 38.57 and 13.47°C, respectively. The simultaneous processes of freshening and cooling compensate each other, leading to an almost constant density (σ = 29.07–29.09 kg m^{-3}). In the three westernmost subregions (VIb, IVb, and VII), the thermohaline properties oscillated without showing further significant trends overcoming the internal variability, indicating that IW cross this area following different paths, leading to a mixture from younger and older IW portions, which are indistinguishable.

For the purposes of our analysis and based on the observed thermohaline differences (a proxy of the age of the IW) data in the subregions Va and Vb have been considered together (V), as opposed to IIa and IIb as well as VIa and VIb, which show strikingly different properties (**Figures 1**, **2B**).

A highly significant trend (U test; $p < 0.0001$) of all biogeochemical properties was observed in IW across the WMED, with the exceptions of SiO_2 and TCO_2 that showed significant ($p < 0.01$) and not significant ($p < 0.5$) changes, respectively, (**Figures 3**, **4**). These changes were due to the concomitant effects of mixing and of biogeochemical processes that take place in the interior of this water mass along its path. The different roles of these two processes will be defined and discussed in section "Role of Mixing and Biological Processes on the Along-Path IW Evolution" where OMP results are used to discriminate them.

Largely positive values of AOU indicate the major effect of the respiration in IW (**Figure 3C**). However, the most important increase of AOU occurs when IW enters and circulates within the Tyrrhenian Sea, from its entrance into this basin (I, IIa) to the exit (IIb or III). Throughout the rest of the path (from IVa onward) AOU remains rather stationary (median values of AOU from 75.1 to 82.9 μmol O_2 kg^{-1}).

From I to VIa, the decrease of TA (median from 2622 to 2592 μmol kg^{-1}; **Figure 3D**) is consistent with the decrease of S (**Figure 3A**). On the other hand, the decrease of pH (from 8.079 to 8.049, **Figure 3E**), along with the contemporary increases of inorganic nutrient concentrations (**Figures 3F–H**) and AOU (**Figure 3C**), suggests an active remineralization of organic matter at intermediate depths. As a result, the concentrations of nutrients in IW showed overall increases from I to VIa by 73% for NO_{3-} (from 4.74 to 8.19 μmol kg^{-1}), 77% for PO_4^{3-} (from 0.211 to 0.37 μmol kg^{-1}) and 26% for SiO_2 (from 4.93 to 6.19 μmol kg^{-1}) (**Figures 3F–H**). In the last three transects (VIb to VII), TA, pH and nutrient concentration show less significant trends.

The along-path pH decrease of the IW induces a shift of the carbonate equilibrium toward more acidic species, with a consequent decrease of the concentration of CO_3^{2-} and an increase of HCO_{3-}, CO_2 and pCO_2 (**Figures 4A–D**). However, the remineralization processes occurring in the intermediate layer while the IW flows through the WMED are not accompanied by a clear increase of TCO_2, which values oscillate at sub-regional scales, with no significant trend ($p < 0.05$) (**Figure 4E**).

Carbonate buffering capacity of IW also decreases as it flows through the WMED, consistently with its progressively less alkaline conditions. The saturation state of calcite (**Figure 4F**)

and aragonite (**Figure 4G**) both decrease from I to VIa (ΩCa goes from 4.48 to 4.01, ΩAr from 2.89 to 2.59), indicating a gradual reduction of the oversaturation of these calcium carbonate minerals along the path. The concomitant increase of the median value of Revelle buffer factor from 10.68 to 11.32 (**Figure 4H**), which quantifies the ocean's sensitivity to an increase in CO_2 (Zeebe and Wolf-Gladrow, 2001; Egleston et al., 2010), indicates that this water mass potentially becomes less efficient to take up CO_2 with aging. Similarly to **Figure 3**, in the last subregions (VIb to VII), there is no significant variation in the parameters of the inorganic carbon system shown in **Figure 4**.

The complete statistics of IW in the electronic (**Supplementary Table S1**) shows the occurrence of high DOC concentrations in the IW at subregion I (median 76.4 μM), compared to VIa–VII (<61.0 μM), as well as the absence of any significant trend along IW pathways for NO_2^-, NH_4^+ and DON.

From a stoichiometric point of view, the evolution of biogeochemical properties along the path of IW from I to VIa corresponds to complex changes of the ratios among biogenic elements (**Table 2**). As already shown, the concentrations of dissolved inorganic nutrients along the IW path constantly increase from I to VIa with an overall mean ratio of NO_3^-:SiO_2:PO_4^{3-} = 18:13:1. The increase of DIN is due to the rise of only NO_3^-, as the concentrations of NO_2^- and NH_4^+ are constant. AOU is linked to nutrient regeneration only in the earliest regions, along the paths I-IIa-IIb and I-IIa-III, despite a relatively high dispersion of AOU data in the transect III (**Figure 3C**). Afterward, AOU values in IW remain high, but also stationary, indicating a decoupling between oxygen consumption and nutrient increase. Changes of DOC and DON were not coupled to those of other parameters, with the exception of a clear inverse correlation between dissolved organic and inorganic carbon pools in the data of the transect I (DOC:TCO_2 = −5.24).

Linear changes in TA and pH are related to changes in salinity and AOU, respectively, indicating the role that mixing and respiration have on these two parameters (**Figures 5A,B**). However, a drop of pH can be observed in the most deoxygenated waters in the transects V and VIa (**Figure 3E**), with low pH values persisting as far as the last subregion (IVb, VIb and VII). The acidification of IW caused a clear shift of the inorganic carbon equilibrium toward the most acidic species (**Figure 4**), but the total concentration of dissolved inorganic carbon did not show an overall trend with respect to oxygen consumption in these subregions (**Figure 5C**). The decrease of pH also caused linear decreases of ΩCa and ΩAr (about −0.1 per 10 μmol O_2 kg^{-1}), with significant negative deviations from linearity down to 4.0 and 2.6, respectively, in VIa (**Figures 5D,E**). The Revelle buffer factor increases from I to VIa (10.6 to 11.3), reaching rather high values that indicate the reduction of the buffering capacity of this water mass, which induces stronger decreases of pH and carbonate ion concentration for a given increase of pCO_2.

In the Menorca-Mallorca region (VIb–VII), hydrological and biogeochemical parameters (**Figure 3**) and carbonate system parameters (**Figure 4**) did not show further clear along-path trends. This most likely indicates that IW may reach this subregion by multiple and variable paths, leading to a complex mixture of younger and older IW portions (**Figure 1**, lower panel). Vertical profiles of the main properties in these 3 transects (**Figure 6**) indicated that IW is located well below the main pycnocline, showing a θ and S range which is encompassed by the variability of DW (**Figures 6A,B**). AOU still reaches the highest values of the whole water column within IW, as a signature of its strong undersaturation, but the difference with the deeper layer is small (**Figure 6C**). Vertical profiles of NO_3^- and PO_4^{3-} indicate that these nutrients show highly variable concentrations within the IW layer (**Figures 6D,E**) in VIb-VII, even though this water mass is located below the main nutriclines of N and P (∼ 200 m). A gradual increase of the concentration with depth is found only for SiO_2, a nutrient that is regenerated slowly in the water column down to the base of the IW layer (>500 m). The ranges of variability of other parameters like DOC, TCO_2, TA and pH also indicate the substantial similarity of the IW characteristics with those of DW (**Figures 6G–K**) in VIb-VII. Saturation states of aragonite (**Figure 6L**) and calcite (not shown) in the IW showed intermediate values between typical AW and DW values, as these parameters usually decrease with depth. For ΩAr, it can also be

TABLE 2 | Linear relationships (slope, standard error, coefficient of determination) among AOU, nutrients and dissolved organic matter in IW, in selected groups of transects of OC2015 cruise.

Parameters	Transects	Ratio y/x (mol/mol)	Slope ± SE (r^2)	Comments
Nutrients	I to VIa	DIN/PO_4^{3-}	17.8 ± 1.0 (*0.823*)	Nutrient increase in IW until VIa with an overall ratio:
	I to VIa	NO_{3-}/PO_4^{3-}	17.8 ± 0.9 (*0.842*)	NO_{3-}:SiO_2:PO_4^{3-} = 18:13:1
	I to VIa	SiO_2/NO_{3-}	0.63 ± 0.06 (*0.580*)	
	I to VIa	SiO_2/PO_4^{3-}	12.5 ± 1.2 (*0.597*)	
	I to III	AOU/DIN	5.0 ± 0.8 (*0.47*)	From IIb to VIa, rather constant values of AOU not related to
	I to III	AOU/NO_3	5.5 ± 0.8 (*0.506*)	changes of nutrient concentration.
	I to III	AOU/PO_4^{3-}	122 ± 12 (*0.686*)	
	I to III	AOU/SiO_2	4.9 ± 0.8 (*0.417*)	
Dissolved organic matter	I to VIa	DOC/DON	–	No relationships along IW path, but high concentrations of DOC in I.
	I to VIa	AOU/DOC	–	
	I to VIa	AOU/DON	–	
	I	DOC/TCO_2	−5.24 ± 0.97 (*0.785*)	No relationships between DOC and TCO_2 in from VIa to VII.

These ratios are the result of the concomitant effects of mixing and biogeochemical processes within the water mass.

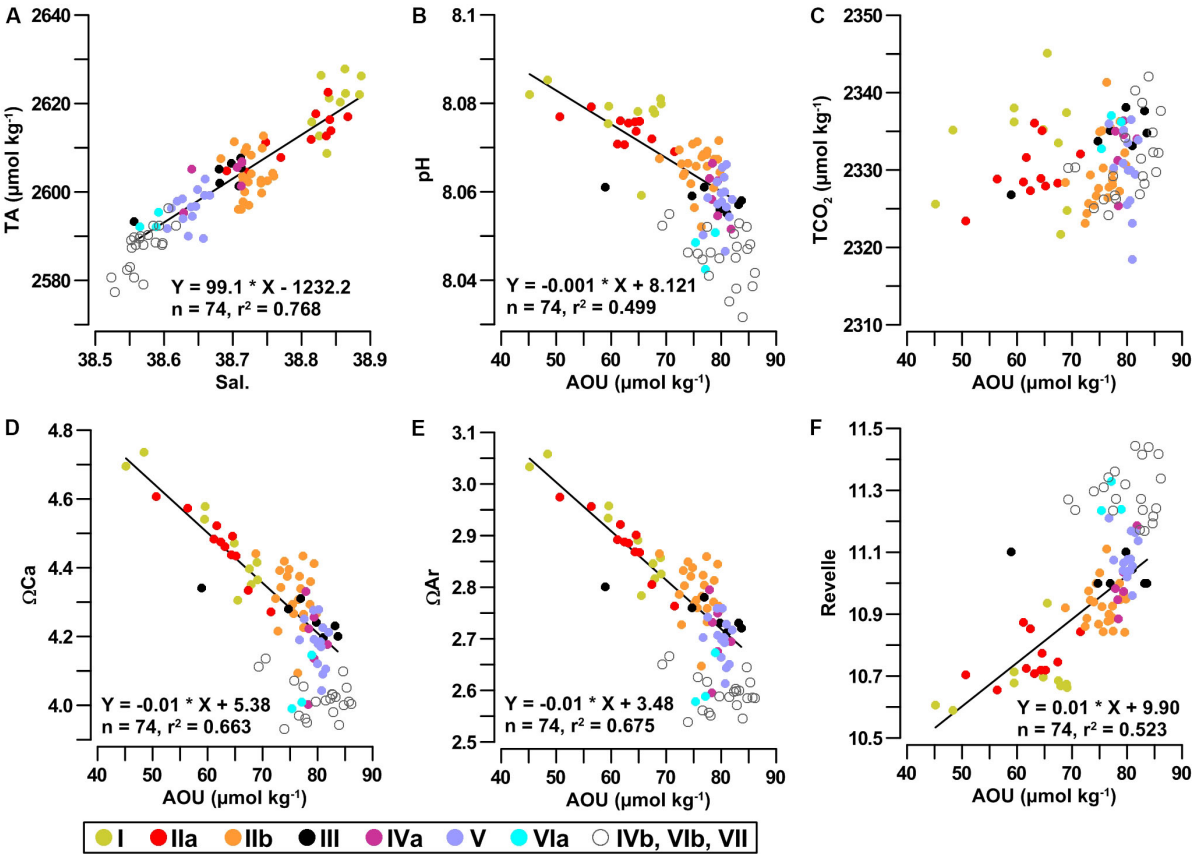

FIGURE 5 | Relationships and linear regressions among *in situ* carbonate system parameters with salinity and AOU in the IW in the subregions from I to VIa. White dots indicate the data of the last three subregions (IVb, VIb and VII). The color code of the dots is the same as in **Figures 1**, **2**. **(A)** TA vs. Salinity, **(B)** pH vs. AOU, **(C)** TCO_2 vs. AOU, **(D)** ΩCa vs. AOU, **(E)** ΩAr vs. AOU, and **(F)** Revelle vs. AOU.

seen that values in IW are always lower than those adequate to an optimal growth of coral reefs (>3.5; Kleypas et al., 1999), but in this subregion they reach the lowest levels of the whole OC2015 cruise (2.5–2.6). To this regard it is worthy to point out that the IW seems to be a key element for the presence of cold water corals (CWCs) in the Mediterranean basin (Orejas and Jiménez, 2019). These authors found that thriving CWC assemblages have a rather punctuated distribution along the circulation path of the IW, which appears to be a main driver for CWC distribution in the Mediterranean (Taviani et al., 2017; Chimienti et al., 2019). Furthermore, The Revelle factor in IW also reaches here the highest level, with a maximum median (11.3) in transect VII.

Biogeochemical data from the interior of IW in VIb, IVb and VII are characterized by the absence of significant correlations between AOU and nutrients, DOC and inorganic carbon, confirming that the remineralization of organic matter is not the major driver in this layer in the Menorca-Mallorca region. The still significant linear relationships among nutrients (NO_3^-:PO_4^{3-} = 24.9, r^2 = 0.84; Si:NO_3^- = 0.7, r^2 = 0.46; DON:NO_3^- = −1.7, r^2 = 0.81) can be mainly explained as the effect of the mixing with nutrient-poor AW and nutrient-rich DW. This effect will be further assessed in section "Role of Mixing and Biological Processes on the Along-Path IW Evolution."

For the inorganic carbon, different property-property ratios were observed in the westernmost Mallorca-Menorca region (**Table 3**, third column), compared to the conditions in the Sicily Channel and southern Tyrrhenian (**Table 3**, second column), which are indicative of an overall transformation along the path through the WMED. The largest decrease of TCO_2 per unitary decrease of TA occurs, and the largest increase of pCO_2 per unitary decrease of pH occurs in this region (slopes of 0.72 and −1305, respectively, vs. 0.62 and −922 in the Sicily Channel and southern Tyrrhenian). By contrast, in these conditions of lower pH in IW, calcite and aragonite saturation states remain low and the Revelle factor remains high, but all these parameters become scarcely dependent on further changes of pH (last three rows of **Table 3**).

Role of Mixing and Biological Processes on the Along-Path IW Evolution

In order to distinguish the importance of the mixing with the surrounding waters and of interior processes in determining the along-path property changes of IW, the mixing of IW with AW and DW was estimated in each subregion by means of the OMP, as described in section "Data Processing and

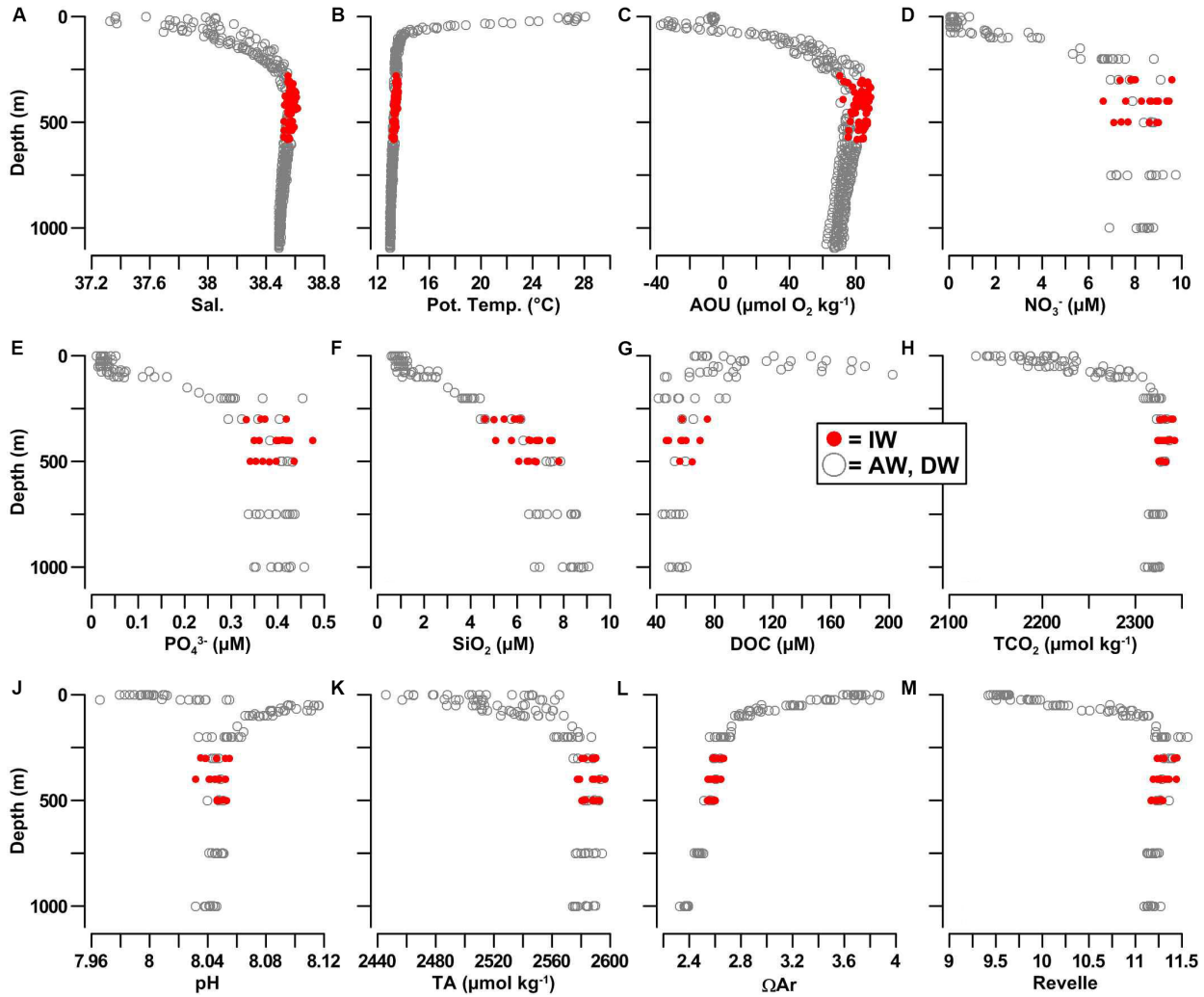

FIGURE 6 | Vertical profiles of *in situ* biogeochemical properties of IW (black dots) in IVb, VIb and VII, compared to the surrounding waters, AW and DW (gray circles). Vertical profiles of **(A)** salinity, **(B)** potential temperature, **(C)** AOU, **(D)** nitrate, **(E)** phosphate, **(F)** silicate, **(G)** DOC, **(H)** TCO_2, **(J)** pH, **(K)** TA, **(L)** ΩAr, and **(M)** Revelle.

TABLE 3 | Slope, standard error and coefficient of correlation (r^2) of the ratios between the *in situ* parameters of inorganic carbon system in IW in the first (I, IIa) and last (Vb, VIb, VII) subregions of OC2015 cruise.

Ratios	Subregions I, IIa Slope ± SE (r^2)	Subregions Vb, IVb, VII Slope ± SE (r^2)
TCO_2/TA	0.62 ± 0.13 (*0.563*)	0.72 ± 0.17 (*0.488*)
HCO_3^-/pH (µmol kg^{-1})	−798 ± 200 (*0.456*)	−793 ± 134 (*0.647*)
CO_3^{2-}/pH (µmol kg^{-1})	530 ± 49 (*0.862*)	344 ± 42 (*0.779*)
pCO_2/pH (µmol kg^{-1})	−922 ± 222 (*0.476*)	−1305 ± 139 (*0.823*)
Revelle/pH	−15.0 ± 1.1 (*0.903*)	−12.6 ± 1.3 (*0.832*)
ΩCa/pH	13.3 ± 4.0 (*0.369*)	5.1 ± 1.7 (*0.326*)
ΩAr/pH	8.6 ± 2.5 (*0.391*)	3.4 ± 1.4 (*0.360*)

Mixing Analysis." Then, following Castro et al. (1998) and Álvarez-Salgado et al. (2014), the relative contribution of mineralization and mixing on the biogeochemical properties previously described can be quantified by applying a multiple correlation to all measured biogeochemical data against the OMP-derived mixing percentages, to establish characteristic values for each water type. Once the WT proportions are calculated with the OMP, it is possible to express any non-conservative parameter as NC = X∗ A + ε, where NC is the matrix of the measured tracer values of every sample, X is the mixing percentages matrix (that resulted from the OMP) and A is the (unknown) corresponding matrix of WT type values for the chemical tracers. ε is the residual matrix that encompasses the non-conservative component of the tracers, the error of the measurement and the non-stationary nature of the properties of the WTs. It is first assumed that the levels of the chemical tracer can be explained only by physical mixing, so that NC_{MIX} = X ∗ A. This equation can be solved for A with a non-negative least squares method, with the condition that all elements of A are ≥0 (Álvarez-Salgado et al., 2014). The results are the WT type values for any tracer that produce the best estimate of the measured

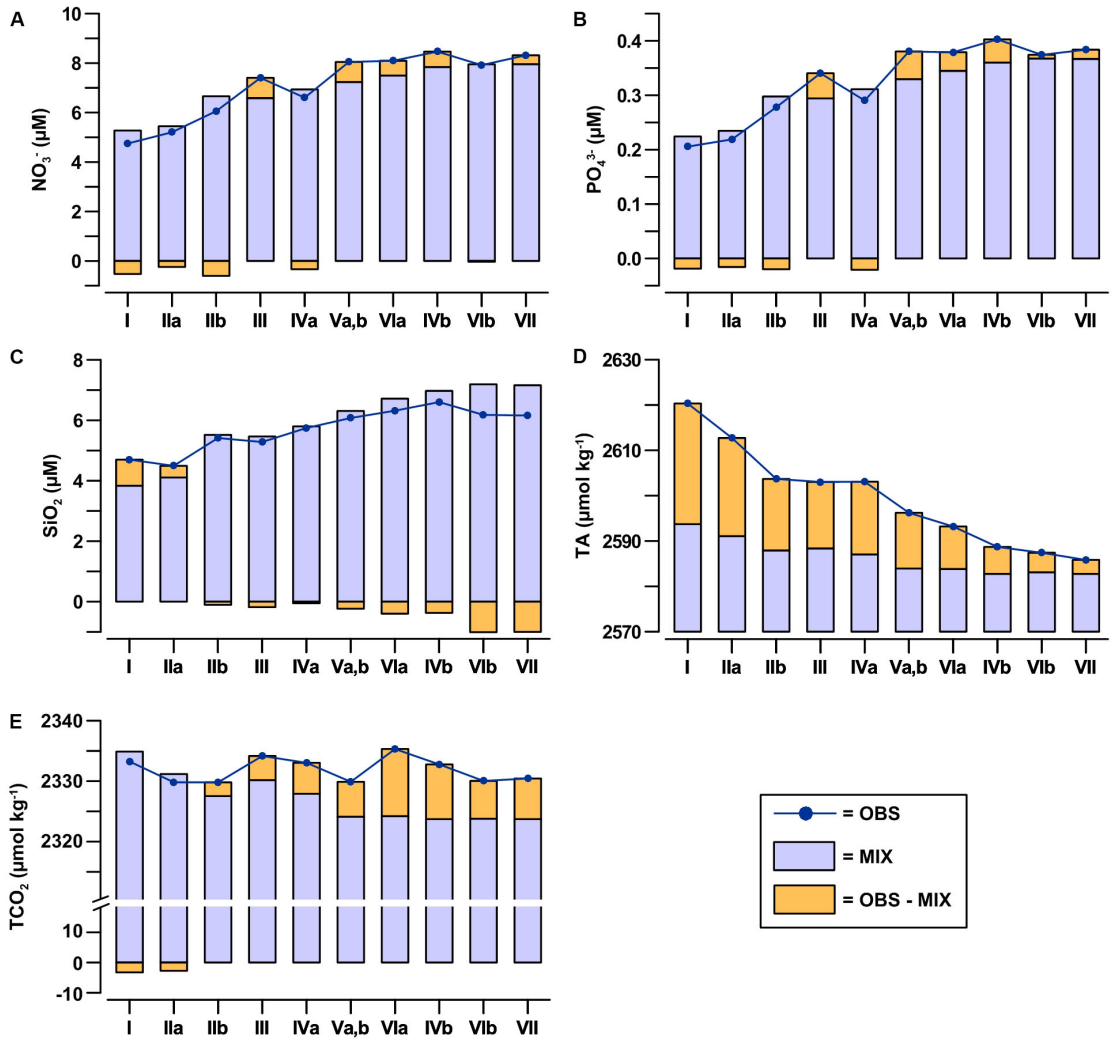

FIGURE 7 | Results of the OMP analysis on major nutrients [**(A)** nitrate, **(B)** phosphate, **(C)** slicate] and *in situ* inorganic carbon [**(D)** TA, **(E)** TCO_2] with respect to the subregion I: observed concentrations in the IW core (OBS), theoretical concentrations derived by OMP (MIX) and differences between observed and theoretical concentrations (OBS–MIX). For the calculation, AW and DW end member concentrations were determined using median values of the layers 100–150 m and 600–1000 m, respectively.

concentrations of the non-conservative tracer (NC_{OBS}), when the WT mixing fractions (X) are multiplied by the WT type values (A). These values in matrix A are a concept close to "preformed concentrations" (Castro et al., 1998; Álvarez-Salgado et al., 2014), but is extended to diluted WTs: thus A includes the variability due to both, the preformed conditions, and the mineralization of biogenic materials from the formation area of each WT to the study area. The difference between the measured tracer level (NC_{OBS}) and the NC_{MIX}, gives us, for each water sample, the contribution of interior non-conservative processes ($NC_{BIO} = NC_{OBS} - NC_{MIX}$).

The relative roles of mixing and biogeochemical processes at the core of IW were analyzed in each transect by comparing median NC_{OBS} and NC_{MIX} concentrations relevant to the layer 150–600 m (**Figure 7**). These differences OBS-MIX indicate that biogeochemical processes have a variable effect in the different transects. The mixing causes a general increase of nutrient concentrations in the intermediate layer (from I to VII), likely due to the generally higher mixing fractions of nutrient-rich DW, with respect to nutrient-poor AW (**Figure 2C**). Non-conservative processes further change nutrient concentrations in the interior of IW. NO_3^- and PO_4^{3-} show common patterns of OBS-MIX (**Figures 7A,B**), with a shift from negative values in the first transects (of the order of −0.6 µM and −0.02 µM, respectively), to positive values in the later transects (of the order of 0.8 µM and 0.05 µM, respectively). These trends indicate an overall enrichment in inorganic nitrogen and phosphorus in IW, due to the remineralization of dissolved and particulate organic matter, which is superimposed to the variability of nutrient levels due to the mixing. The behavior of SiO_2 is the opposite (**Figure 7C**) as it is characterized by a progressive shift from positive (0.9 µM) to negative (−1.0 µM) contribution of

TABLE 4 | Range of the mixing fractions (%) of WT_IW (as defined in **Table 1**) within the layer 150–600 m (values shown in **Figure 2B**) estimated by the OMP analysis, during the different phases of IW evolution.

Phase	Subregion	WT_IW min-max% in IW layer (150–600 m)
1	I	70–93
	IIa	48–90
	IIb	37–76
	III	47–65
2	IVa	48–65
	V	34–53
	VIa	25–40
3	IVb	28–46
	VIb	27–34
	VII	21–44

Max values correspond to the core of IW.

biological processes, which indicates a long-term loss of silicate from the intermediate layer.

Mixing causes a slight decrease of TCO_2 concentration (**Figure 7E**) along the IW path (2335 to 2324 μmol kg^{-1}), due to the negative contribution of the mixing with AW and DW that both have a TCO_2 concentration lower than IW. The lowest TCO_2 concentration is reached in Va,b -VII, where also the mixing fraction of IW is the lowest. The OBS-MIX anomalies of TCO_2, however, indicate that a surplus of dissolved inorganic carbon is generated in the intermediate layer (up to 11 μmol kg^{-1}), due to biological activity, that is consistent with the biologically induced increases of NO_3^- and PO_4^{3-}.

Similarly, to TCO_2, the mixing of IW with the surrounding waters causes a decrease of TA (2594 to 2582 μmol kg^{-1}), which is consistent with the trend of freshening of this water mass observed through the WMED (**Figure 7D**). However, IW shows a significant excess of TA compared to the values that would be generated only by mixing (strongly positive OBS-MIX), which progressively reduces from I to VII. This surplus of TA indicates that, at the entrance in the WMED through the Sicily Channel, IW is more alkaline than any other water mass in the WMED and that its excess in alkalinity is afterward reduced by processes interior to the intermediate layer.

On the whole, property-property relationships (**Figure 5**) and the OMP indicated a prominent effect of respiration to determine the biogeochemical transformations in IW in the regions from I to V, which is gradually masked by mixing in the westernmost region, where sub-regional hydrological conditions seem to play a major role.

DISCUSSION

Data presented in this study indicate that physical and biogeochemical transformations in the IW are strictly connected to the main oceanographic processes in the WMED and that they can be used as a proxy for future evolution that this sea might experience because of regional climate changes.

In this experiment it was possible to intercept the IW flowing into the WMED, at the Sicily Channel, thus when 10 of years already have passed since its formation in the EMED (Schneider et al., 2010). Despite aging and mixing have acted since the formation of this water mass (Lascaratos et al., 1993; Millot and Taupier-Letage, 2005), the thermohaline properties of IW are still very peculiar and well distinguishable in the Sicily Channel, the Sardinian Channel and the Tyrrhenian Sea. Hydrological and biogeochemical considerations, as well as the OMP results, indicate that the evolution of the characteristics of IW in the WMED can be divided into three main phases (**Table 4**, first column):

1. At the beginning of the first phase, IW mainly mixes with AW in the Sicily Channel and the Tyrrhenian entrance, due to the shallowness of these regions. After entering the Tyrrhenian Sea, IW undergoes different mixing processes: (i) the cascading to the bottom of the basin (a process that forms TDW, Sparnocchia et al., 1999) and the consequent vertical mixing with DW and (ii) the diapycnal mixing due to double diffusion in the center of the basin, a peculiar feature of the Tyrrhenian Sea, to which IW contribute as a source of heat and salt (Durante et al., 2019). As a result of these low-energy processes, the fraction of IW at the core of the intermediate layer decreases from 90% at the entrance of the Tyrrhenian basin (IIa) to 76 and 65% in the northern Sardinian Channel (IIb) and the Corsica Channel (III), respectively. In these regions the trends of biogeochemical parameters showed simultaneous increases of AOU and nutrient concentrations, a pH decrease (**Figures 3**, **4**) and an inverse relationship between TCO_2 and DOC at least in transect I, where DOC data were available. These patterns indicate the mineralization of organic matter in the mesopelagic environment, which progressively increases the concentration of the nutrients. The mixing with the surrounding waters is already identifiable in this early phase in the intermediate layer, as shown by freshening and cooling of IW, but it is not a predominant process. The data presented here indicate that a significant refueling of heterotrophic activity occurs in the IW, thanks to the inputs of labile particulate and dissolved organic matter, starting at the time when this water mass crosses the Sicily Channel. Therefore, the high productivity of this marine region (Capodici et al., 2018) appears to be a key-factor for the evolution of biogeochemical properties of IW along the following path in the WMED. Mediterranean heterotrophic communities are well adapted to DOM-poor oligotrophic conditions (Rahav et al., 2019) and they promptly respond to changes of vertical fluxes of phytodetritus from the euphotic layer (Danovaro et al., 2001). Consequently, regional-scale changes in productivity, originated by the alteration of circulation and of seasonal stratification of the water column, are able to change deep-sea ecosystems in the Mediterranean.
2. A second phase of the IW evolution is observed when it crosses the eastern Algero-Provencal Basin, the Ligurian Sea, the Gulf of Lion and the Balearic Sea (IVa to VIa). These areas are important sites of vertical mixing, upwelling and cascading (in winter) of dense shelf waters

with a quite active circulation dynamics, compared to the Tyrrhenian Sea. Along this path, the IW content at the core decreases from 65% to 40%. The biogeochemical evolution was characterized by the decoupling between the different parameters. Along this path, oxygen levels still indicate the persistence of a strong undersaturation in the intermediate layer, but they did not show overall trends from one transect to the next. By contrast, a further mineralization in this water is indicated by the increase of nutrient concentration, with constant ratios and positive OBS-MIX values (**Figure 7**), and by the decrease of pH (**Figure 3E**) that caused a further shift of inorganic carbon equilibria toward acidic species. Considering that constantly low levels of DOC in these subregions does not support a major role of the dissolved organic pool in N- and P-regeneration (**Supplementary Table S1**), inputs of particulate organic matter from the continental shelves might fuel the mineralization in the intermediate layer. These inputs can easily occur during DWF events and cascading of dense shelf waters in the Gulf of Lion and in the Catalan Shelf (The MERMEX Group, 2011). At the same time, the calcification can also contribute to decrease pH and to maintain low oxygen contents.

3. A third phase can be identified in the Menorca – Mallorca region (IVb, IVb, VII), where thermohaline characteristics of IW did not show clear trends from one transect to the next (**Figures 3A,B**). In this region, the presence of multiple paths of circulation and a strong mixing with AW and especially DW (**Figure 2C**) makes it more difficult to distinguish between older and younger IW water parcels. This is the reason why the biogeochemical parameters in the IW did not show further distinct along-path trends, as it can be expected in the presence of a complex circulation of water masses and of a relevant mixing with surrounding waters. The significant role of mixing and mesoscale eddy circulation in this region (Cotroneo et al., 2016) suggests that the characteristics of the Mediterranean outflow in the Atlantic Ocean can be further modified by hydrological transformations in the Alboran Sea. In this region, IW reached the less alkaline conditions, evidenced by a pronounced drop of ΩAr and a rise of the Revelle factor (**Figures 4F–H**), indicating that this water mass is the less adequate to an optimal growth of coral reefs and it has the lowest buffering capacity (Kleypas et al., 1999). In the Menorca–Mallorca region, IW becomes a deoxygenated, nutrient-rich, DOM-poor water mass, whose features are reflected in the outflow of Mediterranean water at the Gibraltar Strait (Voelker et al., 2006).

The stoichiometry of nutrient increases in IW are not far from the oceanic Redfield's model (C:N:Si:P:-O_2 = 105:16:15:1:-172; Takahashi et al., 1985; Pujo-Pay et al., 2011), although they indicate a higher apparent regeneration of NO_3^- compared to SiO_2 and PO_4^{3-}. This deviation can be explained by several processes. A high NO_3^-:PO_4^{3-} ratio in IW can be a signature of the original EMED waters contributing to its formation (Krom et al., 2005). The mixing with the surrounding waters can also modify nutrient ratios in IW, because AW is a PO_4^{3-}-poor water and DW is SiO_2-rich water and the contribution of these two water masses progressively change in the intermediate layer along the WMED (**Figure 2C**). Altered N:P ratios can also result from the activity of heterotrophic communities that persist in the Mediterranean mesopelagic layer, even in the presence of semi-refractory and P-poor organic substrates (Rahav et al., 2019). Moreover, the dissolution of sinking biogenic silica occurs at greater depths, compared to the regeneration of N and P, lowering SiO_2:NO_3^- ratio in IW, as shown by the displacement of the nutriclines during the OC2015 cruise (**Figures 6D–F**). A high consumption of DO with respect to the apparent regeneration of inorganic nutrients is another feature of Mediterranean waters (Bethoux et al., 2005). It is usually thought that high ratios of AOU vs. regenerated nutrients indicate an exhaustive recycling of semi-labile or refractory organic matter in the deeper waters, but these ratios can be also altered by nutrient assimilation by bacteria after their regeneration (Pujo-Pay et al., 2011; Català et al., 2018; Rahav et al., 2019).

On the basis of the OMP adopted in this study, it can be seen that the mixing alone would increase the budgets of the nutrients in IW along its path in the WMED, due to a rising content of nutrient-rich DW and a declining content of nutrient-poor AW in the intermediate layer, from I to VII (**Figures 2C**, **7A–C**). From this point of view, the circulation of IW in the WMED is a mechanism of flushing out of the basin the nutrients that accumulate in the deeper layer. A similar process does not occur for TA and TCO_2, as the mixing reduces both these parameters in the intermediate layer, as AW and DW always have lower concentrations with respect to IW.

The differences between measured tracer concentrations in IW (OBS) and theoretical concentrations originated by mixing (MIX) vary along the IW path, as a function of two distinct factors: (i) the initial content of biogenic elements in IW (i.e. which is a water mass generated in the EMED, outside the realm of the data of OC2015 cruise) with respect to a water mass that would be generated at the same salinity and temperature by the mixing of WMED waters and (ii) the non-conservative processes acting in the interior of IW, when this water mass afterward flows through the WMED.

The initial deficits of NO_3^- and PO_4^{3-} (OBS-MIX in **Figures 7A,B**, transects I-IIa) indicate that the IW entering in the WMED, through the Sicily Channel, is relatively poor in inorganic N and P with respect to a water mass that would be generated by the mixing of WMED waters. This is consistent with the well-known fact that NO_3^- and PO_4^{3-} concentrations in the EMED are generally lower than in the WMED (Pujo-Pay et al., 2011; Krom et al., 2014). owever, a surplus of inorganic N and P is progressively generated in the WMED, by a selective remineralization of these elements in the intermediate layer, a process that is also matched to an increase of the fraction of TCO_2 generated in the interior of IW. The pattern of SiO_2 is the opposite: its initial surplus progressively decreases, due to a loss of SiO_2 from intermediate to deeper waters that overtakes the effect of the mixing. These distinct large-scale pathways of the nutrients confirm the differences between their

cycling in the water column: dissolved and particulate organic N and P are biologically remineralized mostly within of the intermediate layer, whereas the dissolution of sinking biogenic silica mainly occurs in deeper layer (The MERMEX Group, 2011; Krom et al., 2014). In the region of Sicily Channel, TA in IW is also characterized by OBS > MIX (**Figure 7D**), indicating that this water mass entering from the EMED is more alkaline than any other water mass that may be originated by the mixing of WMED waters. This result is consistent with the maximum values of TA measured in the IW of the Ionian Sea (2627 ± 6 μmol kg^{-1}), reported by Álvarez et al. (2014b). Afterward, this excess of TA is reduced (≈ 23 μmol kg^{-1} from I to VII) in the WMED by non-conservative processes. The remineralization of organic matter can concur to reduce this surplus of TA as NO_3^- and PO_4^{3-} regeneration decreases TA (Wolf-Gladrow et al., 2007). A further decrease of TA can be ascribed to carbonate formation ($CaCO_3$ and $MgCO_3$) by calcifying heterotrophic organisms (i.e. planktonic foraminifera and fishes), that decrease TA by 2 moles per 1 mole of precipitate (Wolf-Gladrow et al., 2007). Hence, this process could remove ≈ 10 μmol kg^{-1} of TCO_2 from I to VII, furtherly decoupling the trends of TCO_2 and AOU in this water mass. Calcification, while removing TCO_2, decreases pH and carbonate ion concentration, exerting a synergic effect with organic matter remineralization in determining the observed evolution of these parameters within the IW.

CONCLUSION

The results obtained in this study indicate that hydrological and biogeochemical properties of IW evolve in the WMED under the effect of a variety of forcings, which are likely to change in the future due to climate changes. Consequent alterations of the intermediate layer in the Mediterranean Sea can thus anticipate similar ocean-scale processes global wide.

Along its path through the WMED, the IW undergoes a strong freshening and cooling, due to a gradual mixing with surrounding waters, that decreases its mixing fraction at the core from 93% in the Sicily Channel to 34–46% in the Menorca–Mallorca region. These large variations of thermohaline properties of IW along its path indicate that this water mass is an integrated collector of different physical processes, acting on short/long temporal scales and with high/low energy in the different sub-basins, and that might be differently impacted by long-term climatic trends or by changes in the frequency of extreme events. Climate–driven trends of warming and salinification of surface waters in the EMED (Schroeder et al., 2017; Pastor et al., 2018) affect the process of IW formation, increasing its heat and salt contents. This process might alter the equilibrium depth of IW in the water column, modifying the general water mass stratification and/or changing of the main sites where IW forms. For example, a preferential formation of deeper waters in the EMED, which cannot cross the sill of the Sicily Channel, might increase the importance of other areas, like the Ligurian Sea, for the formation of IW in the WMED. A similar decrease of the inflow of IW into the WMED might also result from a weaker IW formation rate in the EMED, caused by a decrease of surface density and an increase of a persistent stratification of the upper layer that would be typical of a more tropicalized Levantine basin (Somot et al., 2006).

An increase in the frequency of extreme meteorological events is also expected because of the warming of the Mediterranean basin (González-Alemán et al., 2019). This process is potentially able to increase the frequency of short-term/high-energy oceanographic events, like deep convection and cascading, with consequences on the along-path evolution of IW in the WMED. The pathway and turnover time of IW in the WMED strongly influence the mineralization processes occurring within it. Changes originated by chemical and biological modifications of upper waters involved in water mass formation events could easily alter properties and evolution of IW.

It is well known that the Ligurian Sea, the Gulf of Lion and the Catalan Shelf are regions of enhanced vertical dynamics, where dense coastal water can overflow the shelves and cascade down the slope, favoring the transport of particulate matter into the mesopelagic layer (The MERMEX Group, 2011). In particular, submarine canyons constitute a preferential way through which deep-sea environments are exposed to particulate matter fluxes generated by coastal and pelagic productivity (Román et al., 2019) or by the resuspension of sediments (Arjona-Camas et al., 2019). As a result of this vertical mixing, an enhanced reduction in heat and salt contents of IW occurs indicating that, at the end of this part of the path, internal biogeochemical processes are not the major driver of its biogeochemical evolution anymore.

Heterotrophic communities in the mesopelagic environment strongly depend on the production of labile organic matter in the euphotic layer. Changes in the productivity of marine regions crossed by IW, especially the Sicily Channel, may result from climatic alterations having large effects on the biogeochemistry of this water mass. Frequency and intensity of cascading of particulate organic matter generated by pelagic production or by upwelling in marine regions crossed by IW, especially Ligurian Sea, Gulf of Lion and Catalan Shelf, could affect its interior mineralization processes. The metabolism of heterotrophs in the mesopelagic layer also depends on physical conditions, like hydrostatic pressure, currents, salinity and temperature, which are usually characterized by an extremely scarce variability compared to upper waters (Danovaro et al., 2001). However, it has been demonstrated that climate change in the Mediterranean is able to alter these physical constraints in the IW, in particular altering salinity, temperature and equilibrium depth (The MERMEX Group, 2011; Schroeder et al., 2017). In the future, a decrease of calcification rates could be expected in the WMED, as a consequence of the increase of the penetration of anthropogenic CO_2 in the sea. However, the effects on calcifying mesopelagic organisms can hardly be predicted to date, due to the possible concomitant changes of other climatic stressors, like the warming of the water masses (Milner et al., 2016).

Along its path through the WMED, the IW becomes less alkaline and undergoes a significant increase of the Revelle factor in the westernmost region: this indicates that the buffering capacity of IW is greatly reduced while this water mass gets

older, becoming more and more exposed to the adverse effects of a decreasing pH.

DATA AVAILABILITY STATEMENT

Temperature, salinity and dissolved inorganic nutrients data can be downloaded at PANGAEA doi.org/10.1594/PANGAEA.90417 (Belgacem et al., 2019, under review) and doi.pangaea.de/10.1594/PA NGAEA.91104 (Cantoni et al., 2020, under review).

AUTHOR CONTRIBUTIONS

KS and SC wrote the manuscript, prepared the figures, analyzed the dataset. JC coordinated the field work and supervised the writing of the text. CC and APo had the initial idea of the study on intermediate waters and carried out the preliminary data analysis. CC was responsible for the carbonate parameter analysis and did the final editing of the manuscript. CC, SC, Apo, and SD participated to the fieldwork and laboratory analyses. MBe edited the text and suggested some of its structuring, helped to interpret nutrient data. MBo prepared and carried out most of the fieldwork on the ship. SD and APe helped with some specific aspects of the manuscript.

FUNDING

This research has been supported in the framework of the FP 7 Project "OCEAN-CERTAIN Ocean Food-web Patrol – Climate Effects: Reducing Targeted Uncertainties with an Interactive Network" funded by the European Commission (GA #603773).

ACKNOWLEDGMENTS

The authors thank the crew of R/V "Minerva Uno" for the logistic support provided during the oceanographic OC2015 cruise in the Western Mediterranean and the master students Alessandro Cipolla (University of Udine, Italy) and Gianluca Calesso (University of Trieste, Italy) for their help during fieldwork and carbon chemistry analysis. The authors also thank the reviewers for useful suggestions and criticism.

SUPPLEMENTARY MATERIAL

The Supplementary Material for this article can be found online at: https://www.frontiersin.org/articles/10.3389/fmars.2020.00375/full#supplementary-material

REFERENCES

Adloff, F., Somot, S., Sevault, F., Jordà, G., Aznar, R., Déqué, M., et al. (2015). Mediterranean Sea response to climate change in an ensemble of twenty first century scenarios. *Clim. Dyn.* 45, 2775–2802.

Álvarez, M., Brea, S., Mercier, H., and Álvarez-Salgado, X. A. (2014a). Mineralization of biogenic materials in the water masses of the South Atlantic Ocean. I: assessment and results of an optimum multiparameter analysis. *Prog. Oceanogr.* 123, 1–23.

Álvarez, M., Sanleón-Bartolomé, H., Tanhua, T., Mintrop, L., Luchetta, A., Cantoni, C., et al. (2014b). The CO_2 system in the Mediterranean Sea: a basin wide perspective. *Ocean Sci.* 10, 69–92. doi: 10.5194/os-10-69-2014

Álvarez-Salgado, X. A., Álvarez, M., Brea, S., Mčmery, L., and Messias, M. J. (2014). Mineralization of biogenic materials in the water masses of the South Atlantic Ocean. I: stoichiometric ratios and mineralization rates. *Prog. Oceanogr.* 123, 24–37.

Arabic, B. K., and Owens, W. B. (2001). Climatic warming of atlantic intermediate waters. *J. Clim.* 14, 4091–4108.

Arjona-Camas, M., Puig, P., Palanques, A., Emelianov, M., and Durán, R. (2019). Evidence of trawling-induced resuspension events in the generation of nepheloid layers in the Foix submarine canyon (NW Mediterranean). *J. Mar. Syst.* 196, 86–96.

Astraldi, M., Balopoulos, S., Candela, J., Font, J., Gacic, M., Gasparini, G. P., et al. (1999). The role of straits and channels in understanding the characteristics of Mediterranean circulation. *Prog. Oceanogr.* 44, 65–108.

Astraldi, M., and Gasparini, G. P. (1995). "The seasonal characteristics of the circulation in the Tyrrhenian sea," in *Seasonal and Interannual Variability of the Western Mediterranean Sea*, ed. L. Violette (Washington, DC: American Geophysical Union), 115–133.

Belgacem, M., Chiggiato, J., Borghini, M., Pavoni, B., Cerrati, G., Acri, F., et al. (2019). Dissolved inorganic nutrients in the Western Mediterranean Sea (2004–2017). *Earth Syst. Sci.* (in review). doi: 10.5194/essd-2019-136

Benson, B. B., and Krause, D. Jr. (1984). The concentration and isotopic fractionation of oxygen dissolved in freshwater and seawater in equilibrium with the atmosphere. *Limnol. Oceanogr.* 29, 620–632. doi: 10.4319/lo.1984.29.3.0620

Bensoussan, N., Chiggiato, J., Buongiorno, N. B., Pisano, A., and Garrabou, J. (2019). "Insights on 2017 marine heat waves in the Mediterranean Sea," in *Proceedings of the CMEMS Ocean State Report, Issue 3, Journal of Operational Oceanography*, Vol. 12(Suppl. 1), S1–S123. doi: 10.1080/1755876X.2019.1633075

Bethoux, J. P., El Boukhary, M. S., Ruiz-Pino, D., Morin, P., and Copin-Montégut, C. (2005). "Nutrient, oxygen and carbon ratios, CO2 sequestration and anthropogenic forcing in the Mediterranean Sea," in *The Mediterranean Sea. Handbook of Environmental Chemistry*, Vol. 5K, ed. A. Saliot (Berlin: Springer).

Bindoff, N. L., Willebrand, J., Artale, V., Cazenave, A., Gregory, J., Gulev, S., et al. (2007). "Observations: oceanic climate change and sea level," in *Climate Change 2007: The Physical Science Basis. Contribution of Working Group I to the Fourth Assessment Report of the Intergovernmental Panel on Climate Change*, eds S. Solomon, D. Qin, M. Manning, Z. Chen, M. Marquis, K. B. Averyt, et al. (Cambridge: Cambridge University Press).

Cantoni, C., Durante, S., Calesso, G., Cipolla, A., Poiana, A., Borghini, M., et al. (2020). The carbonate chemistry of the Western Mediterranean during the OCEAN CERTAIN 2015 cruise. *PANGAEA* (under review). doi: 10.1594/PANGAEA.911046

Cantoni, C., Luchetta, A., Chiggiato, J., Cozzi, S., Schroeder, K., and Langone, L. (2016). Dense water flow and carbonate system in the southern Adriatic: a focus on the 2012 event. *Mar. Geol.* 375, 15–27. doi: 10.1016/j.margeo.2015.08.013

Capodici, F., Ciraolo, G., Cosoli, S., Maltese, A., Mangano, M. C., and Sarà, G. (2018). Downscaling hydrodynamics features to depict causes of major productivity of Sicilian-Maltese area and implications for resource management. *Sci. Total Environ.* 62, 815–825. doi: 10.1016/j.scitotenv.2018.02.106

Castro, C. G., Pérez, F. F., Holley, S. E., and Rìos, A. F. (1998). Chemical characterisation and modelling of water masses in the Northeast Atlantic. *Prog. Oceanogr.* 42, 249–279.

Català, T. S., Martiïnez-Peìrez, A. M., Nieto-Cid, M., Álvarez, M., Otero, J., Emelianov, M., et al. (2018). Dissolved Organic Matter (DOM) in the open Mediterranean Sea. I. Basin–wide distribution and drivers of chromophoric DOM. *Prog. Oceanogr.* 165, 35–51.

Chiggiato, J., Bergamasco, A., Borghini, M., Falcieri, F. M., Falco, P., Langone, L., et al. (2016). Dense-water bottom currents in the Southern Adriatic Sea in spring 2012. *Mar. Geol.* 375, 134–145.

Chimienti, G., Bo, M., Taviani, M., and Mastrototaro, F. (2019). "Occurrence and biogeography of Mediterranean cold-water corals," in *Mediterranean Cold-Water Corals: Past, Present and Future, Coral Reefs of the World 9*, eds C. Orejas and C. Jiménez (Cham: Springer International Publishing AG).

Clayton, T. D., and Byrne, R. H. (1993). Spectrophotometric seawater pH measurements: total hydrogen ion concentration scale concentration scale calibration of m-cresol purple and at-sea results. *Deep Sea Res. Part I* 40, 2115–2129.

Cotroneo, Y., Aulicino, G., Ruiz, S., Pascual, A., Budillon, G., Fusco, G., et al. (2016). Glider and satellite high resolution monitoring of a mesoscale eddy in the algerian basin: effects on the mixed layer depth and biochemistry. *J. Mar. Syst.* 162, 73–88.

Danovaro, R., Dell'Anno, A., Fabiano, M., Pusceddu, A., and Tselepides, A. (2001). Deep-sea ecosystem response to climate changes: the eastern Mediterranean case study. *Trends Ecol. Evol.* 16, 505–510.

Darmaraki, S., Somot, S., Sevault, F., and Nabat, P. (2019a). Past variability of Mediterranean Sea marine heatwaves. *Geophys. Res. Lett.* 46, 9813–9823. doi: 10.1029/2019GL082933

Darmaraki, S., Somot, S., Sevault, F., Nabat, P., Cabos Narvaez, W. D., Cavicchia, L., et al. (2019b). Future evolution of marine heatwaves in the Mediterranean Sea. *Clim. Dyn.* 53, 1371–1392. doi: 10.1007/s00382-019-04661-z

Dickson, A. G. (1990). Standard potential of the reaction: AgCl(s) þ 1/2H2(g)¼Ag(s) þ HCl(aq), and the standard acidity constant of the ion HSO4 in synthetic seawater from 273.15 to 318.15 K. *J. Chem. Thermodyn.* 22, 113–127.

Dickson, A. G., and Millero, F. J. (1987). A comparison of the equilibrium constants for the dissociation of carbonic acid in seawater media. *Deep Sea Res. Part I* 34, 1733–1743.

Drobinski, P., Da Silva, N., Panthou, G., Bastin, S., Muller, C., Ahrens, B., et al. (2018). Scaling precipitation extremes with temperature in the Mediterranean: past climate assessment and projection in anthropogenic scenarios. *Clim. Dyn.* 51, 1237–1257. doi: 10.1007/s00382-016-3083-x

Duchez, A., Frajka-Williams, E., Josey, S. A., Evans, D. G., Grist, J. P., Marsh, R., et al. (2016). Drivers of exceptionally cold North Atlantic Ocean temperatures and their link to the 2015 European heat wave. *Environ. Res. Lett.* 11:074004.

Durante, S., Schroeder, K., Mazzei, L., Pierini, S., Borghini, M., and Sparnocchia, S. (2019). Permanent thermohaline staircases in the Tyrrhenian Sea. *Geophys. Res. Lett.* 46, 1562–1570. doi: 10.1029/2018GL081747

Egleston, E. S., Sabine, C. L., and Morel, F. M. (2010). Revelle revisited: buffer factors that quantify the response of ocean chemistry to changes in DIC and alkalinity. *Glob. Biogeochem. Cycles* 24:GB1002. doi: 10.1029/2008GB003407

Gačić, M., Lascaratos, A., Manca, B. B., and Mantziafou, A. (2001). "Adriatic deep water and interaction with the Eastern Mediterranean Sea," in *Physical Oceanography of the Adriatic Sea*, eds B. Cushman-Roisin, M. Gačić, P. M. Poulain, and A. Artegiani (Dordrecht: Springer).

Giorgi, F. (2006). Climate change hot−spots. *Geophys. Res. Lett.* 33:L08707. doi: 10.1029/2006GL025734

González-Alemán, J. J., Pascale, S., Gutierrez−Fernandez, J., Murakami, H., Gaertner, M. A., and Vecchi, G. A. (2019). Potential increase in hazard from Mediterranean hurricane activity with global warming. *Geophys. Res. Lett.* 46, 1754–1764. doi: 10.1029/2018GL081253

Grasshoff, K., Ehrhardt, M., and Kremling, K. (1999). *Methods of Seawater Analysis*, 3rd Edn. Weinheim: Verlag Chemie.

Hassoun, A. E. R., Gemayel, E., Krasakopoulou, E., Goyet, C., Saab, M. A. A., Guglielmi, V., et al. (2015). Acidification of the Mediterranean Sea from anthropogenic carbon penetration. *Deep Sea Res. Part I Oceanogr. Res. Pap.* 102, 1–15. doi: 10.1016/j.marenvres.2016.02.016

Hernandez-Ayon, J. M., Belli, S. L., and Zirino, A. (1999). pH, alkalinity and total CO2 in coastal seawater by potentiometric titration with a difference derivative readout. *Ann. Chim. Acta* 394, 101–108.

Huertas, I. E., Ríos, A. F., García-Lafuente, J., Navarro, G., Makaoui, A., and Sánchez-Román, A. (2012). Atlantic forcing of the Mediterranean oligotrophy. *Glob. Biogeochem. Cycles* 26:GB2022. doi: 10.1029/2011GB004167

Kleypas, J. A., McManus, J. W., and Meñez, L. A. B. (1999). Environmental limits to coral reef development: where do we draw the line? *Am. Zool.* 39, 146–159.

Krom, M., Kress, N., Berman-Frank, I., and Rahav, E. (2014). "Past, present and future patterns in the nutrient chemistry of the Eastern Mediterranean," in *The Mediterranean Sea: Its History and Present Challenges*, eds S. Goffredo and Z. Dubinsky (Dordrecht: Springer Netherlands), 49–68.

Krom, M. D., Woodward, E. M. S., Herut, B., Kress, N., Carbo, P., Mantoura, R. F. C., et al. (2005). Nutrient cycling in the south east Levantine basin of the eastern Mediterranean: results from a phosphorus starved system. *Deep Sea Res. Part II Top. Stud. Oceanogr.* 52, 2879–2896.

Lacoue-Labarthe, T., Nunes, P. A. L. D., Ziveri, P., Cinar, M., Gazeau, F., Hall-Spencer, J. M., et al. (2016). Impacts of ocean acidification in a warming Mediterranean Sea: an overview. *Reg. Stud. Mar. Sci.* 5, 1–11. doi: 10.1016/j.rsma.2015.12.005

Lascaratos, A., Williams, R. G., and Tragou, E. (1993). A mixed-layer study of the formation of levantine intermediate water. *J. Geophys. Res.* 14, 739–749.

Lewis, E., and Wallace, D. W. R. (1998). *Program Developed for CO2 System Calculations, ORNL/CDIAC-105*. Oak Ridge, TN: Oak Ridge National Laboratory.

Lionello, P., Malanotte-Rizzoli, P., Boscolo, R., Alpert, P., Artale, V., Li, L., et al. (2006). The Mediterranean climate: an overview of the main characteristics and issues. *Dev. Earth Environ. Sci.* 4, 1–26.

Ludwig, W., Dumont, E., Meybeck, M., and Heussner, S. (2009). River discharges of water and nutrients to the Mediterranean and Black Sea: major drivers for ecosystem changes during past and future decades? *Prog. Oceanogr.* 80, 199–217. doi: 10.1016/j.pocean.2009.02.001

Markaki, Z., Loÿe-Pilot, M. D., Violaki, K., Benyahya, L., and Mihalopoulos, N. (2010). Variability of atmospheric deposition of dissolved nitrogen and phosphorus in the Mediterranean and possible link to the anomalous seawater N/P ratio. *Mar. Chem.* 120, 187–194. doi: 10.1016/j.marchem.2008.10.005

Mehrbach, C., Culberson, C. H., Hawley, J. E., and Pytkowitcz, R. M. (1973). Measurements of the apparent dissociation constants of carbonic acid in seawater at atmospheric pressure. *Limnol. Oceanogr.* 18, 897–907.

Millot, C. (1999). Circulation in the Western Mediterranean Sea. *J. Mar. Syst.* 20, 423–442.

Millot, C. (2013). Levantine Intermediate Water characteristics: an astounding general misunderstanding. *Sci. Mar.* 78, 165–171. doi: 10.3989/scimar.04045.30H

Millot, C., and Taupier-Letage, I. (2005). "Circulation in the Mediterranean Sea," in *The Handbook of Environmental Chemistry*, Vol. 5K, ed. A. Saliot (Berlin: Springer), 29–66.

Milner, S., Langer, G., Grelaud, M., and Ziveri, P. (2016). Ocean warming modulates the effects of acidification on *Emiliania huxleyi* calcification and sinking. *Limnol. Oceanogr.* 61, 1322–1336. doi: 10.1002/lno.10292

Olita, A., Sorgente, R., Natale, S., Gaberšek, S., Ribotti, A., Bonanno, A., et al. (2007). Effects of the 2003 European heatwave on the Central Mediterranean Sea: surface fluxes and the dynamical response. *Ocean Sci.* 3, 273–289. doi: 10.5194/os-3-273-2007

Orejas, C., and Jiménez, C. (eds). (2019). *Mediterranean Cold-Water Corals: Past, Present and Future, Coral Reefs of the World 9*. Cham: Springer International Publishing AG. doi: 10.1007/978-3-319-91608-8_1

Palmiéri, J., Orr, J. C., Dutay, J.-C., Béranger, K., Schneider, A., Beuvier, J., et al. (2015). Simulated anthropogenic CO2 storage and acidification of the Mediterranean Sea. *Biogeosciences* 12, 781–802. doi: 10.5194/bg-12-781-2015

Pastor, F., Valiente, J. A., and Palau, J. L. (2018). Sea surface temperature in the Mediterranean: trends and spatial patterns (1982–2016). *Pure Appl. Geophys.* 175, 4017–4029.

Pujo-Pay, M., Conan, P., Oriol, L., Cornet-Barthaux, V., Falco, C., Ghiglione, J.-F., et al. (2011). Integrated survey of elemental stoichiometry (C, N, P) from the western to eastern Mediterranean Sea. *Biogeosciences* 8, 883–899. doi: 10.5194/bg-8-883-2011

Rahav, E., Silverman, J., Raveh, O., Hazan, O., Rubin-Blum, M., Zeri, C., et al. (2019). The deep water of Eastern Mediterranean Sea is a hotspot for bacterial activity. *Deep Sea Res. Part II* 164, 135–143. doi: 10.1016/j.dsr2.2019.03.004

Roether, W., Manca, B. B., Klein, B., Bregant, D., Georgopoulos, D., Beitzel, V., et al. (1996). Recent changes in Eastern Mediterranean deep waters. *Science* 271, 333–335.

Román, S., Ortiz-Álvarez, R., Romano, C., Casamayor, E. O., and Martin, D. (2019). Microbial community structure and functionality in the Deep Sea floor: evaluating the Causes of Spatial heterogeneity in a submarine canyon system (NW Mediterranean, Spain). *Front. Mar. Sci.* 6:108. doi: 10.3389/fmars.2019.00108

Schneider, A., Tanhua, T., Kortzinger, A., and Wallace, D. W. R. (2010). High anthropogenic carbon content in the eastern Mediterranean. *J. Geophys. Res.* 115:C12050. doi: 10.1029/2010JC006171

Schneider, A., Tanhua, T., Roether, W., and Steinfeldt, R. (2014). Changes in ventilation of the Mediterranean Sea during the past 25 year. *Ocean Sci.* 10, 1–16.

Schroeder, K., Chiggiato, J., Bryden, H. L., Borghini, M., and Ben Ismail, S. (2016). Abrupt climate shift in the Western Mediterranean Sea. *Sci. Rep.* 6:23009. doi: 10.1038/srep23009

Schroeder, K., Chiggiato, J., Josey, S. A., Borghini, M., Aracri, S., and Sparnocchia, S. (2017). Rapid response to climate change in a marginal sea. *Sci. Rep.* 7:4065. doi: 10.1038/s41598-017-04455-5

Schroeder, K., Garcìa-Lafuente, J., Josey, S. A., Artale, V., Buongiorno Nardelli, B., and Carrillo, A. (2012). "Chapter 3: circulation of the Mediterranean Sea and its variability," in *The Climate of the Mediterranean Region, from the Past to the Future*, ed. P. Lionello (Amsterdam: Elsevier Insights).

Schroeder, K., Gasparini, G. P., Borghini, M., Cerrati, G., and Delfanti, R. (2010). Biogeochemical tracers and fluxes in the Western Mediterranean Sea, spring 2005. *J. Mar. Syst.* 80, 8–24. doi: 10.1016/j.jmarsys.2009.08.002

Schroeder, K., Gasparini, G. P., Tangherlini, M., and Astraldi, M. (2006). Deep and intermediate water in the Western Mediterranean under the influence of the Eastern Mediterranean transient. *Geophys. Res. Lett.* 33:L21607. doi: 10.1029/2006GL027121

Schroeder, K., Taillandier, V., Vetrano, A., and Gasparini, G. P. (2008). The circulation of the Western Mediterranean Sea in spring 2005 as inferred from observations and from model outputs. *Deep Sea Res. Part I* 55, 947–965.

Sisma-Ventura, G., Yam, R., Kress, N., and Shemesh, A. (2016). Water column distribution of stable isotopes and carbonate properties in the South-eastern Levantine basin (Eastern Mediterranean): vertical and temporal change. *J. Mar. Syst.* 158, 13–25. doi: 10.1016/j.jmarsys.2016.01.012

Somot, S., Sevault, F., and Déqué, M. (2006). Transient climate change scenario simulation of the Mediterranean Sea for the twenty-first century using a high-resolution ocean circulation model. *Clim. Dyn.* 27, 851–879.

Sparnocchia, S., Gasparini, G. P., Astraldi, M., Borghini, M., and Pistek, P. (1999). Dynamics and mixing of the Eastern Mediterranean outflow in the Tyrrhenian basin. *J. Mar. Syst.* 20, 301–317.

Stöven, T., and Tanhua, T. (2014). Ventilation of the Mediterranean Sea constrained by multiple transient tracer measurements. *Ocean Sci.* 10, 439–457. doi: 10.5194/os-10-439-2014

Stratford, K., Williams, R., and Drakopoulos, P. (1998). Estimating climatological age from a model derived oxygen−age relationship in the Mediterranean. *J. Mar. Syst.* 18, 215–226.

Takahashi, T., Broecker, W. S., and Anger, S. (1985). Redfield ratio based on chemical data from isopycnal surfaces. *J. Geophys. Res.* 90, 6907–6924.

Taviani, M., Angeletti, L., Canese, S., Cannas, R., Cardonee, F., Cauda, A., et al. (2017). The "Sardinian cold-water coral province" in the context of the Mediterranean coral ecosystems. *Deep Sea Res. Part* 2, 61–78. doi: 10.1016/j.dsr2.2015.12.008

Testor, P., Bosse, A., Houpert, L., Margirier, F., Mortier, L., Legoff, H., et al. (2018). Multiscale observations of deep convection in the Northwestern Mediterranean Sea during winter 2012-2013 using multiple platforms. *J. Geophys. Res. Oceans* 123, 1745–1776. doi: 10.1002/2016JC012671

The MERMEX Group (2011). Marine ecosystems' responses to climatic and anthropogenic forcings in the Mediterranean. *Prog. Oceanogr.* 91, 97–166.

Tomczak, M., and Large, D. G. B. (1989). Optimum multiparameter analysis of mixing in the thermocline of the eastern Indian Ocean. *J. Geophys. Res.* 94, 16141–16149.

Toucanne, S., Jouet, G., Ducassou, E., Bassetti, M.-A., Dennielou, B., Angue Minto'o, C. M., et al. (2012). A 130,000-year record of levantine intermediate water flow variability in the Corsica Trough, western Mediterranean Sea. *Quat. Sci. Rev.* 33, 55–73.

Touratier, F., Goyet, C., Houpert, L., Madron, X. D., and De Lefčvre, D. (2016). Deep-Sea Research I Role of deep convection on anthropogenic CO_2 sequestration in the Gulf of Lions (northwestern Mediterranean Sea). *Deep Sea Res. Part I* 113, 33–48. doi: 10.1016/j.dsr.2016.04.003

Uppström, L. R. (1974). The boron/chloronity ratio of deep-seawater from the Pacific Ocean. *Deep Sea Res.* 21, 161–162.

Voelker, A., Lebreiro, S., Schonfeld, J., Cacho, I., Erlenkeuser, H., and Abrantes, F. (2006). Mediterranean outflow strengthening during northern hemisphere coolings: a salt source for the glacial Atlantic? *Earth Planet. Sci. Lett.* 245, 39–55. doi: 10.1016/j.epsl.2006.03.014

Wolf-Gladrow, D. A., Zeebe, R. E., Klaas, C., Körtzinger, A., and Dickson, A. G. (2007). Total alkalinity: the explicit conservative expression and its application to biogeochemical processes. *Mar. Chem.* 106, 287–300.

Zeebe, R. E., and Wolf-Gladrow, D. (2001). *CO2 in Seawater: Equilibrium, Kinetics, Isotopes. Elsevier Oceanography Series*, Vol. 65. Amsterdam: Elsevier, 346.

Conflict of Interest: The authors declare that the research was conducted in the absence of any commercial or financial relationships that could be construed as a potential conflict of interest.